

FIELD TOLERANCES ASSOCIATED WITH SOME
RESONANCES IN THE TRIUMF CYCLOTRON

by

JEAN LOUIS BOLDUC

B.A., Laval University, 1965
B.Sc.A., Laval University, 1969

A thesis submitted in partial fulfilment of
the requirements for the degree of

Master of Science

in the Department
of
Physics

We accept this thesis as conforming to the
required standard

THE UNIVERSITY OF BRITISH COLUMBIA
April, 1972

In presenting this thesis in partial fulfilment of the requirements for an advanced degree at the University of British Columbia, I agree that the Library shall make it freely available for reference and study. I further agree that permission for extensive copying of this thesis for scholarly purposes may be granted by the Head of my Department or by his representatives. It is understood that copying or publication of this thesis for financial gain shall not be allowed without my written permission.

Department of PHYSICS

The University of British Columbia
Vancouver 8, Canada

Date 14th April 1972

ABSTRACT

This thesis is concerned with tolerances for magnetic field imperfections in the TRIUMF cyclotron set by the betatron oscillation resonances $\nu_x = 1.0$, $\nu_x - \nu_z = 1.0$ and $\nu_x = 1.5$. These resonances, encountered during acceleration, can lead to undesirable growth in the amplitudes of the betatron oscillations.

We first derive equations of motion that take into account non-linear terms and field imperfections, and show how resonance conditions may occur. These conditions were simulated in our orbit codes and numerical calculations were made to determine the tolerances they impose on the magnetic field.

We have made a detailed investigation of the effect on the behaviour of the beam of first harmonic bumps at radii less than 150 in. The first harmonic tolerance of 0.1 G to produce an increase in the radial amplitude of 0.1 in. is in agreement with analytical calculations. We have also shown that this tolerance, too small to be seen in the magnetic field survey, may be achieved by suitable adjustments in the harmonic coil settings. Tolerances on the second harmonic imperfection are also presented.

To determine the tolerances set by the coupled resonance $\nu_x - \nu_z = 1.0$, we have simulated a first harmonic twist in the median plane. The results show that, for high current poor resolution experiments, the magnitude of the twist on entering the resonance is of no importance, provided the amplitudes of the radial and vertical betatron oscillations are not much larger than the estimate of 0.2 in. For high resolution experiments, the tolerances on the slope of the twist are of the order of a few mrad. Analytical estimates of these tolerances are also presented.

Finally, we have determined that the $\nu_x = 1.5$ resonance sets an upper limit to the gradient of the third harmonic of about 0.2 G/in., which produces a 20% increase in the radial betatron amplitude.

TABLE OF CONTENTS

	Page
1. INTRODUCTION	1
2. MATHEMATICAL DESCRIPTION	4
2.1 Equations of Motion	4
2.1.1 Introduction	4
2.1.2 Linear Dynamics	4
2.1.3 Non-Linear Dynamics	7
2.2 Resonances	11
3. THE CENTRAL REGION	16
3.1 Introduction	16
3.2 Sensitivity to a First Harmonic	16
3.2.1 Introduction	16
3.2.2 Calculations	18
3.3 Harmonic Coils	22
3.3.1 Oscillatory First Harmonic	22
3.3.2 Ions with a Wide Range of RF Phases	28
4. THE RESONANCE $\nu_x - \nu_z = 1$	45
4.1 Mathematical Description	45
4.2 Calculations	48
4.3 Tolerances	56
5. THE RESONANCE $\nu_x = 1.5$	58
5.1 The Intrinsic Resonance $\nu_x = 6/4$	58
5.2 The Resonance $\nu_x = 3/2$	61
5.2.1 Introduction	61
5.2.2 Calculations	63
5.2.3 Static and Accelerated Phase Space with Third Harmonic Gradient	66
References	72
Appendix A. Magnetic Field Components in the Plane of Measurement	73

LIST OF TABLES

	Page
1.1 Total energy spread	2
3.1 Betatron amplitudes for 0 deg RF phase ions	24
3.2 Betatron amplitudes with harmonic coil field	27
3.3 Components of displacements due to first harmonic of Fig. 3.8	33
3.4 Coefficients for set of coils at $37'' \leq R \leq 54''$	33
3.5 Coefficients for set of coils at $54'' \leq R \leq 71''$	34
3.6 Coefficients for set of coils at $71'' \leq R \leq 89''$	34
3.7 Harmonic coil correcting fields	35
3.8 Displacements for ideal orbit due to first harmonic of Fig. 3.8	36
3.9 Displacements from ideal orbit when first harmonic error and correcting fields are present	36
3.10 Displacements of the equilibrium orbit centre due to first and second imperfection harmonics of 1 G and 2 G, respectively, for ions of 0 deg RF phase at 1 MeV and $v_x = 1.001$	43
3.11 Displacements of the equilibrium orbit centre due to first and second imperfection harmonics of 1 G and 2 G, respectively, for ions of 0 deg RF phase at 3 MeV and $v_x = 1.004$	43
4.1 Maximum betatron amplitudes (either x_{final} or z_{final}) below and above the resonance $v_x - v_z = 1$ when $v_x \approx 1.2$ and $v_z \approx 0.2$	56

LIST OF FIGURES

	Page
2.1 Plot of v_x versus v_z , for field 01/30/10/70	14
3.1 Phase space for accelerated ions (0.8 MeV to 28 MeV) of 0 deg RF phase with various first harmonics present	20
3.2 The amplitude of a 20 in. wide first harmonic bump required to produce radial betatron amplitudes of 0.2 in.	21
3.3 Residual first harmonic obtained from superposition of harmonic coil field corrections to first harmonic error field	23
3.4 Profile of oscillatory first harmonic	25
3.5 Bump profile	25
3.6 Positions at 35 MeV for ions of 0 deg RF phase accelerated from low energy	26
3.7 Phases and amplitudes of the oscillations produced by standard harmonic coil field and by first harmonic error	30
3.8 Profile of first harmonic error	30
3.9 Displacements from "ideal" centre point at 35 MeV due to a 2 G field in each set of coils, for ions of 0 deg, 25 deg and 40 deg RF phase	32
3.10 Phase space plot for accelerated ions (1 MeV to 35 MeV) of 0 deg RF phase with both the first harmonic error and the harmonic coil correcting fields present	38
3.11 Phase space plot for accelerated ions (1 MeV to 35 MeV) of 40 deg RF phase with both the first harmonic error and the harmonic coil correcting fields present	39
3.12 Phase space plot for accelerated ions (1 MeV to 35 MeV) of 30 deg RF phase with both the first harmonic error and the harmonic coil correcting fields present	40
3.13 Limits of radial stability for second harmonic error field	42
4.1 Section view of the cyclotron median plane with tilted median plane parameters	50
4.2 Static phase space ellipse at 153 MeV corresponding to a radial betatron amplitude of 0.25 in.	50
4.3 Radial and vertical betatron oscillations at 153 MeV (on resonance) when a first harmonic twist with a slope of $\alpha = 0.02$ rad and $R_0 = \bar{R}_{153}$ MeV is present	52

	Page	
4.4	Radial and vertical betatron oscillations at 144 MeV (10 MeV below resonance) when a first harmonic twist with a slope of $\alpha = 0.02$ rad and $R_0 = \bar{R}_{144}$ MeV is present	53
4.5	Radial and vertical betatron oscillations at $125 \text{ MeV} \leq E \leq 153 \text{ MeV}$ when a first harmonic twist with a slope of $\alpha = 0.02$ rad and $R_0 = \bar{R}_{153}$ MeV is present	55
5.1	Phase space plot at 425 MeV and $\nu_x = 1.487$ for ions of 0 deg phase (resonance $\nu_x = 6/4$)	59
5.2	Unstable fixed-points motion for field 01/18/02/70	60
5.3	Unstable fixed-points motion for field 02/09/07/71	62
5.4	The effect of the bump phase parameter on the width of the resonance in the case of a 0.4 G/in. third harmonic gradient with $R_s = 287.5$ in.	64
5.5	The effect of the starting radius parameter on the width of the resonance in the case of a 0.4 G/in. third harmonic gradient with $\phi_3 = \phi_6 + 15$ deg	64
5.6	The effect of various gradient amplitudes on the width of the resonance when $R_s = 287.5$ in. and $\phi_3 = \phi_6 + 15$ deg	65
5.7	Phase space plot of 430 MeV and $\nu_x = 1.492$ for ions of 0 deg RF phase when a 0.5 G/in. third harmonic gradient is present	67
5.8	Effective phase space area occupied by the beam at 441 MeV when no third harmonic gradient is present	69
5.9	Effective phase space area occupied by the beam at 441 MeV when a third harmonic gradient of 0.2 G/in. amplitude is present	69
5.10	Effective phase space area occupied by the beam at 441 MeV when a third harmonic gradient of 0.4 G/in. amplitude is present	70
A.1	Tilted magnet sector parameters	75

ACKNOWLEDGEMENTS

I am much indebted to Dr. G.H. Mackenzie for his invaluable help in directing this research.

Thanks are also due to Dr. M.K. Craddock, Dr. W. Joho and Dr. M.M. Gordon for helpful suggestions and to Miss Colleen Meade for her assistance with the computer programs.

I also wish to thank Miss Ada Strathee for her work in typing this thesis.

This research was made possible by a scholarship and a bursary from the National Research Council of Canada.

1. INTRODUCTION

The TRIUMF cyclotron¹ is designed to accelerate negative hydrogen ions up to an energy of approximately 500 MeV. The H⁻ ions are produced in an external ion source and guided, through the injection system, down the axis of the cyclotron into their first orbit. Then a two-dee system with a dee-to-dee peak voltage of 200 kV, giving an energy gain per turn of 400 keV, is used to reach the desired energy.

During its acceleration, the particle oscillates about an equilibrium position, in both the radial and the vertical direction. This equilibrium orbit is defined as an orbit, in the median plane of the cyclotron, with the same 6-fold symmetry as the magnetic field; that is, an orbit that closes on itself after each sector. The motion about the equilibrium orbit is analogous, in first approximation, to the motion of a two-dimensional harmonic oscillator. The Hamiltonian for this system may be written

$$H = \frac{1}{2} \left(\nu_x^2 x^2 + p_x^2 \right) + \frac{1}{2} \left(\nu_z^2 z^2 + p_z^2 \right) \quad (1.1)$$

where (x, p_x) and (z, p_z) are the displacements in position and momentum, in the radial and vertical direction respectively, from the equilibrium orbit. The ν_x and ν_z are, respectively, the number of radial and vertical oscillations per turn. The corresponding equations of motion are

$$x'' + \nu_x^2 x = 0 \quad (1.2)$$

$$z'' + \nu_z^2 z = 0 \quad (1.3)$$

where the primes represent the derivation with respect to θ , the azimuth around the machine. Then, to this approximation, the ion describes two independent sinusoidal betatron oscillations about the equilibrium orbit.

In order to achieve good energy resolution at extraction, the amplitudes of these betatron oscillations must remain small. Table 1.1 illustrates the relation between the total energy spread at two energies and the amplitude of the radial oscillation A_x .

A_x at 30 MeV (in.)	0.14	0.25	0.40
200 MeV	1.0	1.2	1.6
500 MeV	1.2	1.8	2.4

Table 1.1 Total energy spread (MeV)

Stability is achieved if the beam is properly focused both radially and vertically. In the radial direction, focusing is always achieved since, for any isochronous cyclotron with three or more sectors, such as TRIUMF, the value of ν_x is approximately given by $\nu_x \approx \gamma$ where $\gamma = 1 + \tau/mc^2$, τ being the kinetic energy of the ion of rest mass m . Therefore, ν_x starts at unity and increases afterwards; the beam is then contained in that direction. In the vertical direction, the field flutter, which is a measure of the change in field strength between the hills and the valleys, provides an axial force known as the Thomas force,² which is always focusing. Two additional forces, discovered by Kerst and Laslett,³ also contribute to the axial focusing. Both forces depend on the spiral shape of the magnet sector. Their effect is alternately focusing and defocusing. However, because of the alternating gradient principle and because of different path lengths in the focusing and defocusing fields, their net effect is focusing.

Once we achieve the conditions for axial and vertical focusing, the next problem is to avoid resonances. We call "resonance" a situation in

which the amplitude of the radial or the vertical oscillation grows with θ , the azimuth around the machine. Some of the resonances are intrinsic and are due to non-linearities in the equations of motion, neglected in Eqs. 1.2 and 1.3. Others come from mechanical imperfections such as misalignment or magnetic non-uniformity of the magnet sectors. In the next chapters, we will first derive more accurate expressions for the equations of motion and show how resonance conditions may occur. We will then look at some particular cases of resonances encountered in the operation of the TRIUMF cyclotron and determine the tolerances they impose on the magnetic field.

2. MATHEMATICAL DESCRIPTION

2.1 Equations of Motion

2.1.1 Introduction

A system of cylindrical co-ordinates (r, θ, z) is used to describe the radial and vertical motion of a particle with relativistic mass m and charge q in a magnetic field \vec{B} . The force applied to the particle is

$$\vec{F} = q \vec{v} \times \vec{B} \quad (2.1)$$

where

$$\vec{v} = (\dot{r}, r\dot{\theta}, \dot{z}) \quad (2.2)$$

is the velocity of the particle and where the dots represent the derivative with respect to time. From Lagrange's equations, we obtain

$$\frac{d}{dt}(m\dot{r}) - mr\dot{\theta}^2 = q(r\dot{\theta}B_z - \dot{z}B_\theta) \quad (2.3)$$

$$\frac{d}{dt}(m\dot{z}) = q(\dot{r}B_\theta - r\dot{\theta}B_r). \quad (2.4)$$

Using these two equations, Walkinshaw and King⁴ derived linear expressions for the radial and vertical motion. We summarize most of their calculations in the following section, and then extend them to consider qualitatively some non-linear effects.

2.1.2 Linear Dynamics

Since the particle velocity along the orbit is constant we may transform the independent variable from time t to θ , the azimuth around the machine. Walkinshaw and King assume that $(r'/r)^2$, $(z'/r)^2$ and $(r'z'/r^2)$ are all much less than unity and that the term in $\dot{z}B_\theta$ is unlikely to be important. Then, the equation for the radial motion in the median plane may be written

$$r'' - r = \frac{q}{mv} r^2 B_z \quad (2.5)$$

where the primes denote differentiation with respect to the new variable θ . Similarly, the equation for the vertical motion takes the form

$$z'' + \frac{q}{mv} (r^2 B_r - r r' B_\theta) = 0. \quad (2.6)$$

We assume a perfectly flat median plane and, since $\text{curl} \vec{B} = 0$ in a static magnetic field, we may write to a linear approximation in z

$$B_z = B = \left(B_z \right)_{z=0} \quad (2.7)$$

$$B_r = z \frac{\partial B}{\partial r}$$

$$B_\theta = z \frac{1}{r} \frac{\partial B}{\partial \theta}.$$

Eq. 2.6 becomes

$$z'' + \frac{q}{mv} \left(r^2 \frac{\partial B}{\partial r} - r' \frac{\partial B}{\partial \theta} \right) z = 0. \quad (2.8)$$

We then define a reference circle of radius r_0 , the equilibrium radius in the homogeneous magnetic field, by the condition $r_0 = \frac{mv}{qB_0}$, where B_0 is the azimuthally averaged value of B at r_0 . Writing $R = r/r_0$, Eqs. 2.5 and 2.8 become

$$\frac{d^2 R}{d\theta^2} - R = R^2 \frac{B}{B_0} \quad (2.9)$$

$$\frac{d^2 z}{d\theta^2} + \left[R^2 \frac{\partial}{\partial R} (B/B_0) + \frac{\partial R}{\partial \theta} \cdot \frac{\partial}{\partial \theta} (B/B_0) \right] z = 0. \quad (2.10)$$

The next step is to derive the equations for the radial and vertical oscillations of the particle around the equilibrium orbit. For the vertical motion we assume, in first approximation, that the radial

motion is confined to the equilibrium orbit, i.e. $R = R_{eo}(\theta)$, where $R_{eo}(\theta) = 1 + \rho(\theta)$ is the radius of the closed orbit. We write

$$\frac{d^2z}{d\theta^2} + \left(R_{eo}^2 \frac{\partial}{\partial R} (B/B_0) \Big|_{R_{eo}} + \frac{\partial R_{eo}}{\partial \theta} \cdot \frac{\partial}{\partial \theta} (B/B_0) \right) z = 0. \quad (2.11)$$

For the radial motion we expand R about the equilibrium orbit, i.e.

$R = R_{eo} + x$. We also write the field (B/B_0) as a Taylor's series about its value on the equilibrium orbit. To a linear approximation in x ,

Eq. 2.9 becomes

$$\frac{d^2x}{d\theta^2} + \left(-1 + \frac{1}{B_0} \left[-\frac{\partial (R^2 B)}{\partial R} \right]_{R_{eo}} \right) x = 0. \quad (2.12)$$

Then, a Fourier analysis of $B(\theta)$ makes Eq. 2.11 and Eq. 2.12 of Mathieu Hill form. When the harmonic terms are small, the resulting equations can be reduced to the form of Eq. 1.2 and Eq. 1.3, provided we are interested only in the motion per turn (i.e. $n = \theta/2\pi$ becomes the new independent variable) and not in the detailed motion in each sector.

In the following, we will assume for simplicity that the radial and vertical oscillations have been smoothed out into a sinusoidal motion of constant angular frequency, ν_x and ν_z , respectively. In this case, the particle precesses along an ellipse in the (x, p_x) or (z, p_z) phase space. In practice, however, the non-sinusoidal character of the oscillation makes the particle move along a slightly different curve. We have shown that, in TRIUMF, the discrepancy from the ideal case in the radial motion is always less than 25% of the betatron amplitude, in the region of maximum flutter. This is acceptable for our present purpose.

Eqs. 2.11 and 2.12 would then describe these two independent sinusoidal oscillations.

2.1.3 Non-Linear Dynamics

More generally, the radial and vertical betatron oscillations, as well as magnet imperfections, will cause higher order terms and coupling terms between the two motions to be introduced in the equations of motion. These higher order terms, added to the right-hand side of Eqs. 2.11 and 2.12, will transform our free oscillations into forced oscillations. The main feature of these forced oscillations is that instability may arise because of a resonance condition between the frequency of the free oscillation and the frequency of the perturbing force. This happens when the perturbation term oscillates with the frequency of the free oscillation or with any of its integral multiples.

To illustrate the various types of resonances, we first expand our previous expressions for the magnetic field to include quadratic terms in z . In the case of a flat median plane, Eq. 2.7 becomes

$$B_z = B - \frac{z^2}{2r_0^2} \nabla^2 B \quad (2.13)$$

$$B_R = \frac{z}{r_0} \frac{\partial B}{\partial R}, \quad B_\theta = \frac{z}{r_0} \frac{1}{R} \frac{\partial B}{\partial \theta}$$

where B is again written for the z -component of the magnetic field in the median plane and

$$\nabla^2 = \frac{\partial^2}{\partial R^2} + \frac{1}{R} \frac{\partial}{\partial R} + \frac{1}{R^2} \frac{\partial}{\partial \theta^2} \quad (2.14)$$

is the Laplacian in polar co-ordinates R, θ . We also consider a small deviation from the ideal 6-fold symmetric isochronous field; we write

$$B = B_i + \Delta B \quad (2.15)$$

where B_i includes the sixth harmonic of the magnetic field and its

multiples and where ΔB may also be expressed as a Fourier series and contains the "imperfection" harmonics. Similarly, because of magnet imperfections, we no longer assume a symmetric median plane, so that our z -co-ordinate is changed according to $z = z + z_0$. We assume that z_0 is small compared to the dimensions of the magnet, and we write

$$z_0 = \sum_{n=0}^{\infty} \sum_{p=0}^{\infty} \epsilon_{n,p} x^n \cos(p\theta + \phi_p). \quad (2.16)$$

In the following, we set the phases ϕ_p equal to zero degree. In all the cases we consider the perturbations in the guiding field are periodic functions of θ with a period of $2\pi/p$. Then, the field imperfections can be analysed in a Fourier series. We consider only the p^{th} Fourier component, such that p is an integer.

Because of the median plane asymmetry, new terms must be added to the expressions of the magnetic field components; for small values of z_0 , Eq. 2.13 becomes (see Appendix A)

$$B_z = B - \frac{z}{r_0^2} \nabla^2 (z_0 B) - \frac{z^2}{2r_0^2} \nabla^2 B \quad (2.17)$$

$$B_R = \frac{1}{r_0} \left(z \frac{\partial B}{\partial R} + \frac{\partial (z_0 B)}{\partial R} \right)$$

$$B_\theta = \frac{1}{r_0} \left(\frac{z}{R} \frac{\partial B}{\partial \theta} + \frac{1}{R} \frac{\partial (z_0 B)}{\partial \theta} \right).$$

Also, the term in $\dot{z}B_\theta$ of Eq. 2.3 is no longer neglected. Then, with the use of Eq. 2.17, Eq. 2.3 and Eq. 2.4 may be rewritten as

$$R'' - R = \frac{R^2}{B_0} \left(B - \frac{z}{r_0^2} \nabla^2 (z_0 B) - \frac{z^2}{2r_0^2} \nabla^2 B \right) - \frac{z'}{B_0 r_0^2} \left(z \frac{\partial B}{\partial \theta} + \frac{\partial (z_0 B)}{\partial \theta} \right) \quad (2.18)$$

$$z'' + \frac{1}{B_0} \left(R^2 \frac{\partial B}{\partial R} - R' \frac{\partial B}{\partial \theta} \right) z = - \frac{R^2}{B_0} \frac{\partial (z_0 B)}{\partial R} + \frac{R'}{B_0} \frac{\partial (z_0 B)}{\partial \theta}. \quad (2.19)$$

The assumption that the harmonic terms are small is maintained in the following calculations. For the radial motion we expand R about the equilibrium orbit and express B_i and ΔB as Taylor's series in x . From Eq. 2.18 we obtain

$$\begin{aligned}
 x'' + v_x^2 x &= R_{eo}^2 \frac{\Delta B}{B_0} + 2x R_{eo} \frac{\Delta B}{B_0} + x \frac{R_{eo}^2}{B_0} \frac{\partial(\Delta B)}{\partial R} - z \frac{R_{eo}^2}{r_0^2 B_0} \nabla^2(z_0 B_i) \\
 &+ x^2 \left(\frac{B_i}{B_0} + \frac{2R_{eo}}{B_0} \frac{\partial B_i}{\partial R} + \frac{R_{eo}^2}{2B_0} \frac{\partial^2 B_i}{\partial R^2} \right) - z^2 \frac{R_{eo}^2}{2r_0^2 B_0} \nabla^2 B_i \\
 &- z' \frac{1}{r_0^2 B_0} \frac{\partial(z_0 B_i)}{\partial \theta} - z z' \frac{1}{r_0^2 B_0} \frac{\partial B_i}{\partial \theta}. \tag{2.20}
 \end{aligned}$$

where we kept only up to second order terms in x , z , z_0 and ΔB . We then use Eq. 2.16 to include contributions due to deviation from a flat median plane. To a second order expansion in x , z , ΔB and $\epsilon_{n,p}$, we obtain

$$\begin{aligned}
 x'' + v_x^2 x &= R_{eo}^2 \frac{\Delta B}{B_0} + 2x R_{eo} \frac{\Delta B}{B_0} + x \frac{R_{eo}^2}{B_0} \frac{\partial(\Delta B)}{\partial R} - z \left(\frac{R_{eo}^2}{r_0^2 B_0} \nabla^2 B_i \epsilon_{0,p} \cos p\theta \right. \\
 &- \left. \frac{p^2 B_i}{r_0^2 B_0} \epsilon_{0,p} \cos p\theta + \frac{R_{eo}}{r_0^2 B_0} B_i \epsilon_{1,p} \cos p\theta + \frac{2R_{eo}^2}{r_0^2 B_0} B_i \epsilon_{2,p} \cos p\theta \right) \\
 &+ x^2 \left(\frac{B_i}{B_0} + \frac{2R_{eo}}{B_0} \frac{\partial B_i}{\partial R} + \frac{R_{eo}^2}{2B_0} \frac{\partial^2 B_i}{\partial R^2} \right) - z^2 \frac{R_{eo}^2}{2r_0^2 B_0} \nabla^2 B_i \\
 &- z' \left(\frac{p B_i}{r_0^2 B_0} \epsilon_{0,p} \sin p\theta - \frac{1}{r_0^2 B_0} \frac{\partial B_i}{\partial \theta} \epsilon_{0,p} \cos p\theta \right) - z z' \frac{1}{r_0^2 B_0} \frac{\partial B_i}{\partial \theta}. \tag{2.21}
 \end{aligned}$$

where the p refers to the harmonics of the twist in the median plane.

In the case of the vertical motion, we assumed previously that the radial motion was confined to the equilibrium orbit. Since the particle executes radial betatron oscillations, we must expand R about the equilibrium orbit in Eq. 2.19. We also include the deviation 2.15 from the ideal

field, and we obtain

$$\begin{aligned}
 z'' + v_z^2 z &= -\frac{R_{e0}^2}{B_0} \frac{\partial(z_0 B_i)}{\partial R} - \frac{R_{e0}^2}{B_0} \frac{\partial(z_0 \Delta B)}{\partial R} + \frac{\partial R_{e0}}{\partial \theta} \frac{1}{B_0} \frac{\partial(z_0 B_i)}{\partial \theta} \\
 &+ \frac{\partial R_{e0}}{\partial \theta} \frac{1}{B_0} \frac{\partial(z_0 \Delta B)}{\partial \theta} - z \left(\frac{R_{e0}^2}{B_0} \frac{\partial(\Delta B)}{\partial R} - \frac{\partial R_{e0}}{\partial \theta} \frac{1}{B_0} \frac{\partial(\Delta B)}{\partial \theta} \right) \\
 &- 2x \frac{R_{e0}}{B_0} \frac{\partial(z_0 B_i)}{\partial R} + x' \frac{1}{B_0} \frac{\partial(z_0 B_i)}{\partial \theta} \\
 &+ 2zx \frac{R_{e0}}{B_0} \frac{\partial B_i}{\partial R} + zx' \frac{1}{B_0} \frac{\partial B_i}{\partial \theta} . \tag{2.22}
 \end{aligned}$$

Then, with Eq. 2.16 our final expression becomes

$$\begin{aligned}
 z'' + v_z^2 z &= -\frac{R_{e0}^2}{B_0} \frac{\partial B_i}{\partial R} \epsilon_{0,p} \cos p\theta - \frac{R_{e0}^2}{B_0} B_i \epsilon_{1,p} \cos p\theta - \frac{R_{e0}^2}{B_0} \frac{\partial(\Delta B)}{\partial R} \epsilon_{0,p} \cos p\theta \\
 &+ \frac{R_{e0}^2}{B_0} \Delta B \epsilon_{1,p} \cos p\theta + \frac{1}{B_0} \frac{\partial R_{e0}}{\partial \theta} \frac{\partial B_i}{\partial \theta} \epsilon_{0,p} \cos p\theta \\
 &- \frac{p}{B_0} \frac{\partial R_{e0}}{\partial \theta} B_i \epsilon_{0,p} \sin p\theta + \frac{1}{B_0} \frac{\partial R_{e0}}{\partial \theta} \cdot \frac{\partial(\Delta B)}{\partial \theta} \epsilon_{0,p} \cos p\theta \\
 &- \frac{p}{B_0} \frac{\partial R_{e0}}{\partial \theta} \Delta B \epsilon_{0,p} \sin p\theta - z \left(\frac{R_{e0}^2}{B_0} \frac{\partial(\Delta B)}{\partial R} - \frac{1}{B_0} \frac{\partial R_{e0}}{\partial \theta} \cdot \frac{\partial(\Delta B)}{\partial \theta} \right) \\
 &- x \left(\frac{R_{e0}^2}{B_0} \frac{\partial B_i}{\partial R} \epsilon_{1,p} \cos p\theta + \frac{2R_{e0}^2}{B_0} B_i \epsilon_{2,p} \cos p\theta \right. \\
 &+ \frac{2R_{e0}}{B_0} \frac{\partial B_i}{\partial R} \epsilon_{0,p} \cos p\theta + \frac{2R_{e0}}{B_0} B_i \epsilon_{1,p} \cos p\theta \\
 &\left. - \frac{1}{B_0} \frac{\partial R_{e0}}{\partial \theta} \cdot \frac{\partial B_i}{\partial \theta} \epsilon_{1,p} \cos p\theta + \frac{p}{B_0} \frac{\partial R_{e0}}{\partial \theta} B_i \epsilon_{1,p} \cos p\theta \right) \\
 &+ x' \left(\frac{1}{B_0} \frac{\partial B_i}{\partial \theta} \epsilon_{0,p} \cos p\theta - \frac{p B_i}{B_0} \epsilon_{0,p} \sin p\theta + \frac{1}{B_0} \frac{\partial R_{e0}}{\partial \theta} B_i \epsilon_{1,p} \cos p\theta \right) \\
 &- 2zx \frac{R_{e0}}{B_0} \frac{\partial B_i}{\partial R} + zx' \frac{1}{B_0} \frac{\partial B_i}{\partial \theta} . \tag{2.23}
 \end{aligned}$$

where we neglected terms of the third and higher orders in z , x , ΔB and $\epsilon_{n,p}$. Eq. 2.21 and Eq. 2.23 describe the forced oscillations of the particle in the radial and vertical direction. We can now investigate the various intrinsic resonances due to non-linearities as well as resonances due to magnet imperfections.

2.2 Resonances

The simplest case of resonance arises when an exterior interference force due to a perturbation in the field amplitude is added to our free oscillation. Considering only the first term on the right-hand side of Eq. 2.21, we expand ΔB in a Fourier series and we select the p^{th} component. Then Eq. 2.21 is written

$$x'' + \nu_x^2 x = \frac{R_{e0}^2}{B_0} B_p \cos p\theta \quad (2.24)$$

where B_p is the amplitude of the perturbation in the magnetic field. The solution of the homogeneous part of Eq. 2.21 is given by

$$x = A_x \cos(\nu_x \theta + \phi) \quad (2.25)$$

where A_x is the amplitude of the radial oscillation. Then, the right-hand side of Eq. 2.24 will oscillate with the same frequency ν_x whenever

$$\nu_x = p \quad (2.26)$$

i.e. when ν_x is an integer. Similarly, by adding only the third term on the right-hand side of Eq. 2.21 to our free oscillation, we may write

$$x'' + \nu_x^2 x = x \frac{R_{e0}^2}{B_0} \frac{\partial B_p}{\partial R} \cos p\theta. \quad (2.27)$$

We then use first order perturbation theory to replace x in the right-hand side of Eq. 2.27 by the solution 2.25, and we transform the product

of harmonics into a sum. We find that resonances occur when

$$\nu_x = p/2. \quad (2.28)$$

While the *integral resonances* are sensitive to a flat harmonic error, the *half-integral resonances* are primarily driven by gradient errors in the guiding field. From Eq. 2.23 we see that resonances due to gradient imperfections also appear in the vertical motion; similarly, the integral resonances appear when a twist in the median plane is present.

The misalignment of the median plane may, on the other hand, introduce linear coupling terms in both the radial and the vertical motion. Keeping only the first term in x on the right-hand side of Eq. 2.23, we write

$$z'' + \nu_z^2 z = -x \frac{R^2}{B_0} \frac{\partial B_z}{\partial R} \epsilon_{1,p} \cos p\theta. \quad (2.29)$$

We then replace x on the right-hand side of Eq. 2.29 by the solution of the radial free oscillation, and we find that *linear coupled resonances* occur when

$$\nu_x \pm \nu_z = p. \quad (2.30)$$

This type of resonance may arise from the term proportional to $z\nabla^2 B_z$ in Eq. 2.21; the driving harmonic is the p^{th} harmonic of the slope of the twist in the median plane. A corresponding coupling term is found in the equation for the radial motion.

We consider finally the *non-linear resonances*. Some of those resonances arise from magnet errors, others are intrinsic resonances due to non-linear terms in the equations of motion. The general case of a non-linear term may be written as

$$\text{coupling term} = \varepsilon x^{n-1} z^m \cos p\theta \quad (2.31)$$

where we chose $(n-1)$ rather than n for greater simplicity in the final expression. The equation for the radial motion becomes

$$x'' + v_x^2 x = \varepsilon x^{n-1} z^m \cos p\theta \quad (2.32)$$

$$x'' + v_x^2 x = \varepsilon \cos^{n-1} v_{x\theta} \cos^m v_{z\theta} \cos p\theta. \quad (2.33)$$

Transforming the product of harmonic functions into a sum, we find that the condition for resonance is fulfilled if

$$n v_x \pm m v_z = p \quad (2.34)$$

where $n, m, p=0, \pm 1, \pm 2, \dots$. The odd values of m correspond to median plane errors since they arise only, in the radial motion, from the expression 2.16. Eq. 2.34 contains all the previous types of resonances, namely resonances 2.26, 2.28 and 2.30. We can show that Eq. 2.34 may be obtained from a driving term like $\varepsilon x^n z^{m-1} \cos p\theta$ in the vertical motion.

Some of the resonances described by Eq. 2.34 are schematically shown in Fig. 2.1. The horizontal and vertical lines correspond to integral and half-integral resonances, while the other straight lines correspond to coupled resonances. We call $|n| + |m| = N$ the order of the resonance. It is easily seen, from the expressions 2.32 and 2.34, that a resonance of order N is driven, in first order, by a term of order $(N-1)$ in the equations of motion. The driving harmonic is the p^{th} Fourier component of the field or magnet imperfection. It has been shown by Sturrock⁵ that, in most cases, dangerous instabilities arise only if n and m are of the same sign, i.e. when we have a "sum resonance". Furthermore,⁶ if $|n| + |m| \geq 4$, the motion is usually stable. Finally, although we have

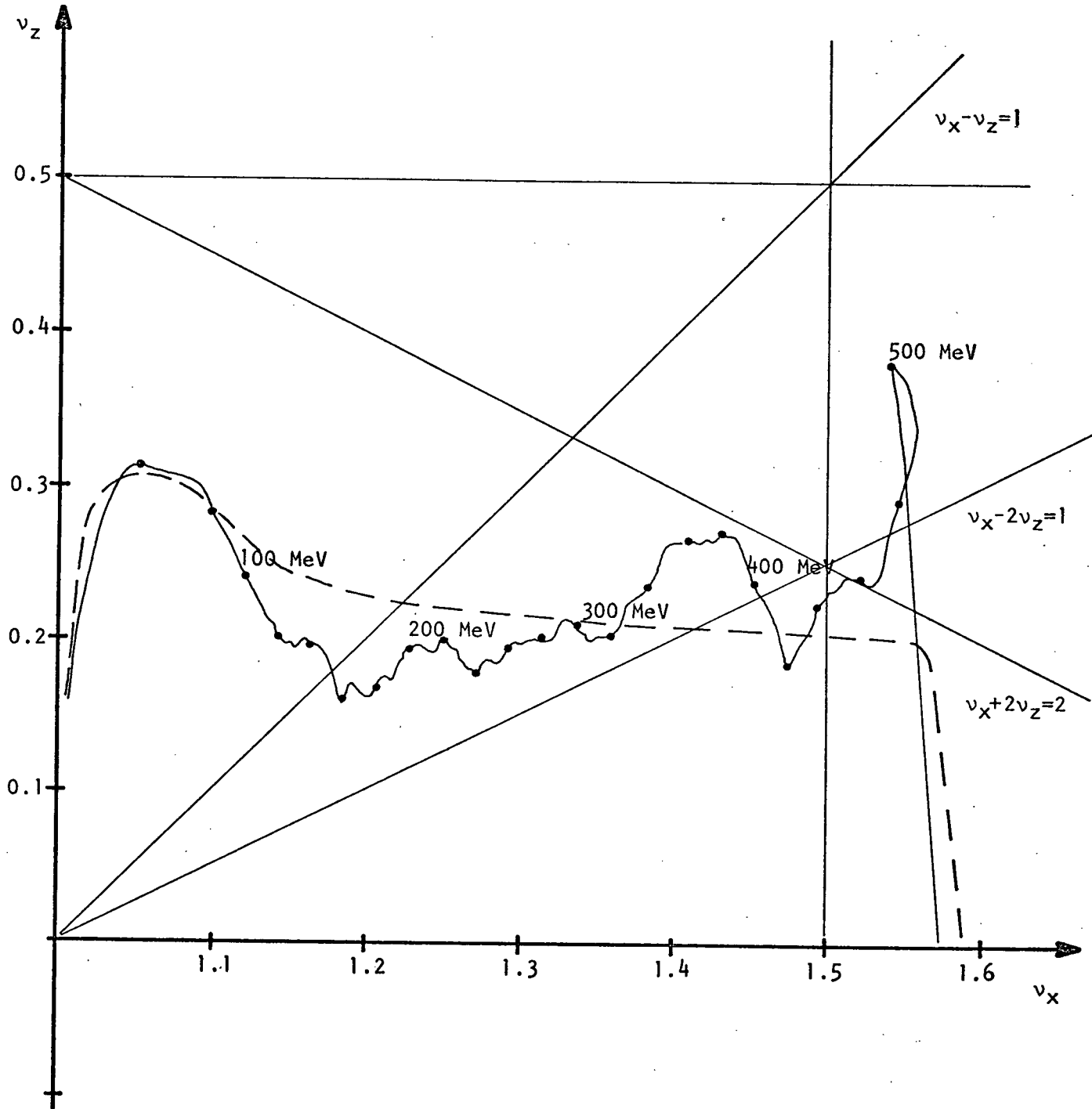


Fig. 2.1. Plot of v_x versus v_z , for field 01/30/10/70

drawn lines on Fig. 2.1, Sturrock has pointed out that the resonances can cause increases in the betatron oscillation amplitudes over regions extending some distance on either side of these lines.

The dashed line on Fig. 2.1 represents the expected values, for TRIUMF, of ν_z versus ν_x after shimming, while the dotted line shows the working path for field 01/30/10/70 before shimming. We observe that, at low energies, the value of the frequency for the radial betatron oscillation is close to one. Similarly, we cross the coupled resonance $\nu_x - \nu_z = 1$ around 150 MeV and, at higher energies, we cross the resonance $\nu_x = 1.5$. These three regions are sensitive to field or to magnet imperfections and will be discussed in more detail in the following chapters.

3. THE CENTRAL REGION

3.1 Introduction

In the central portion of the cyclotron the resonance $\nu_x = 1.0$ is driven, in first order, by a first harmonic imperfection. The first harmonic is superimposed on the dominant terms in the Fourier expansion of the magnetic field, namely the sixth harmonic and its multiples. In general, the effect of the imperfection is to increase the amplitude of the radial oscillation. We set our tolerances according to the maximum acceptable value of this betatron oscillation. The limit is introduced from considerations on beam quality, such as the energy resolution. The second harmonic can also drive the resonance $\nu_x = 1.0$ but its effect is less important. We will, however, consider both imperfections.

3.2 Sensitivity to a First Harmonic

3.2.1 Introduction

A general analysis of the effects of first harmonic field errors on the radial oscillations has been made by Lawson.⁷ However, an approximate treatment can be obtained using the following simple procedure. The equation for the radial motion in the presence of a first harmonic forcing term may be written

$$x'' + \nu_x^2 x = b_1 \cos(\theta + \phi_1) \quad (3.1)$$

where x is the radial displacement from the equilibrium orbit in units of the orbit radius, b_1 is the amplitude of the forcing term, i.e. the ratio of the amplitude of the first harmonic B_1 to the average field \bar{B} , and ϕ_1 is the azimuth of the peak of the driving harmonic. The general solution of Eq. 3.1 is

$$x = \frac{b_1}{(\nu_x^2 - 1)} \cos(\theta + \phi_1) + A \cos(\nu_x \theta + \psi). \quad (3.2)$$

The particle precesses in a circular path about an equilibrium orbit centre displaced by a distance d_1 , in inches, given by

$$d_1 = \frac{R_{e0} B_1}{B(\nu_x^2 - 1)} \quad (3.3)$$

where R_{e0} is the radius of the equilibrium orbit we consider and ν_x is the frequency of the radial oscillation at that radius. When $(\nu_x - 1)$ is small, the ion bunch will precess slowly about this displaced orbit centre and, after N turns, the bunch will be displaced by a distance d^* where

$$d^* = 2d_1 \sin\left[\pi(\nu_x - 1)N\right] \approx 2\pi N d_1(\nu_x - 1). \quad (3.4)$$

If the first harmonic bump is suddenly turned off after the N^{th} turn, d^* will be the coherent betatron amplitude which we call A_x . In other words, a step first harmonic bump of B_1 gauss between radii R_A and R_B will produce a betatron oscillation amplitude of

$$A_x = \frac{\pi N (R_A + R_B) B_1}{B(\nu_x + 1)}. \quad (3.5)$$

This assumes that ν_x is constant between R_A and R_B ; N is the number of turns made between R_A and R_B . In fact, a step-shaped first harmonic is not realistic for TRIUMF; the steepest rise or fall that we would expect is from 10% to 90% of maximum values in about 10 in., or half the magnet gap width. However, Eq. 3.5 is still a useful approximation if only a small portion of the precession cycle is made while the first harmonic amplitude is changing. This is true when $(\nu_x - 1)$ is small.

For a continuous field error, where the amplitude of the imperfection harmonic is constant with radius, Lawson⁷ has derived a formula for

the corresponding amplitude of the betatron oscillation. He obtained

$$a_x = 0.65 \left(\frac{4\pi}{\epsilon} \right)^{\frac{1}{4}} r_\infty \frac{B_1}{B} \quad (3.6)$$

where $r_\infty = \frac{c}{\omega}$ is the cyclotron unit of length and ϵ is the ratio of the energy gain per turn to the ion rest energy.

3.2.2 Calculations

These were performed using the code GOBLIN and the field 1/07/04/70. All calculations assumed that only the fundamental RF frequency was present, no third harmonic. When the third harmonic is present, ions of different phases get more nearly the same energy gain per turn and hence acquire similar betatron amplitudes.

We first determined the "ideal path" for ions in (x, p_x) phase space by running GOBLIN backwards from 50 MeV to low energy to get approximate starting conditions. We then ran forwards, adjusting the starting conditions so that ions of 0 deg RF phase had no large cusps or loops in their phase space path and ended up on centre in a 6-fold field at 50 MeV. This gave us our standard starting co-ordinates for forward runs. We regarded residual wiggles of about 0.05 in. amplitude as acceptable.

We then superimposed our field imperfections and observed the path in (x, p_x) space of an ion starting at the standard co-ordinates with 0 deg RF phase. At some energy, beyond the influence of the imperfection, the ions would be precessing in phase space in circles of roughly constant diameter. The displacement from the ideal path, at a particular energy, was considered to be the betatron amplitude gained from resonance. It was found to be almost linearly proportional to the first harmonic amplitude and almost independent of its phase. This can be seen on Fig. 3.6 where a

bump of 0.2 G builds up an oscillation of 0.09 in. amplitude while a bump of 0.4 G produces an oscillation of 0.19 in.

Fig. 3.1 illustrates some results obtained in the two cases we studied. The first was for a first harmonic whose amplitude was uniform with radius; an amplitude of 0.2 G produced a radial amplitude of 0.20 in. compared with the 0.18 in. predicted by Eq. 3.6. The other case was for a bell-shaped bump with a half-width of 20 in. Fig. 3.1 shows the results when the bumps were centred at 30 in. The field bump of 0.5 G builds up an oscillation of 0.15 in. while our previous Eq. 3.5 predicted an amplitude of 0.13 in. Similarly, the 2.0 G bump produces an oscillation of 0.65 in.

We have made a detailed investigation of the effect of first harmonic bumps at radii less than 150 in. on the behaviour of the beam. We used the fact of linearity to get more accurate results with larger bumps so that the 0.05 in. residual oscillation of the "ideal case" was negligible. Fig. 3.2 shows the results of these calculations in the form of the amplitude of a bell-shaped first harmonic bump 20 in. wide placed at different radii and necessary to produce a betatron amplitude of 0.2 in.; this was considered to be the worst that could be accepted. The results show that the most sensitive region is that around 60 in. where a bump of 0.2 G produces an oscillation of 0.2 in. of amplitude. This last result is approximately equal to the amplitude gained from a continuous field error.

The behaviour of the field strength can be understood by considering the motion of the centre points. We have seen that when $(v_x - 1)$ is small the ion bunch precesses slowly about the displaced equilibrium orbits. The amplitude acquired is given by Eq. 3.5. At very low energies, the lack of

FIELD 01/07/04/70

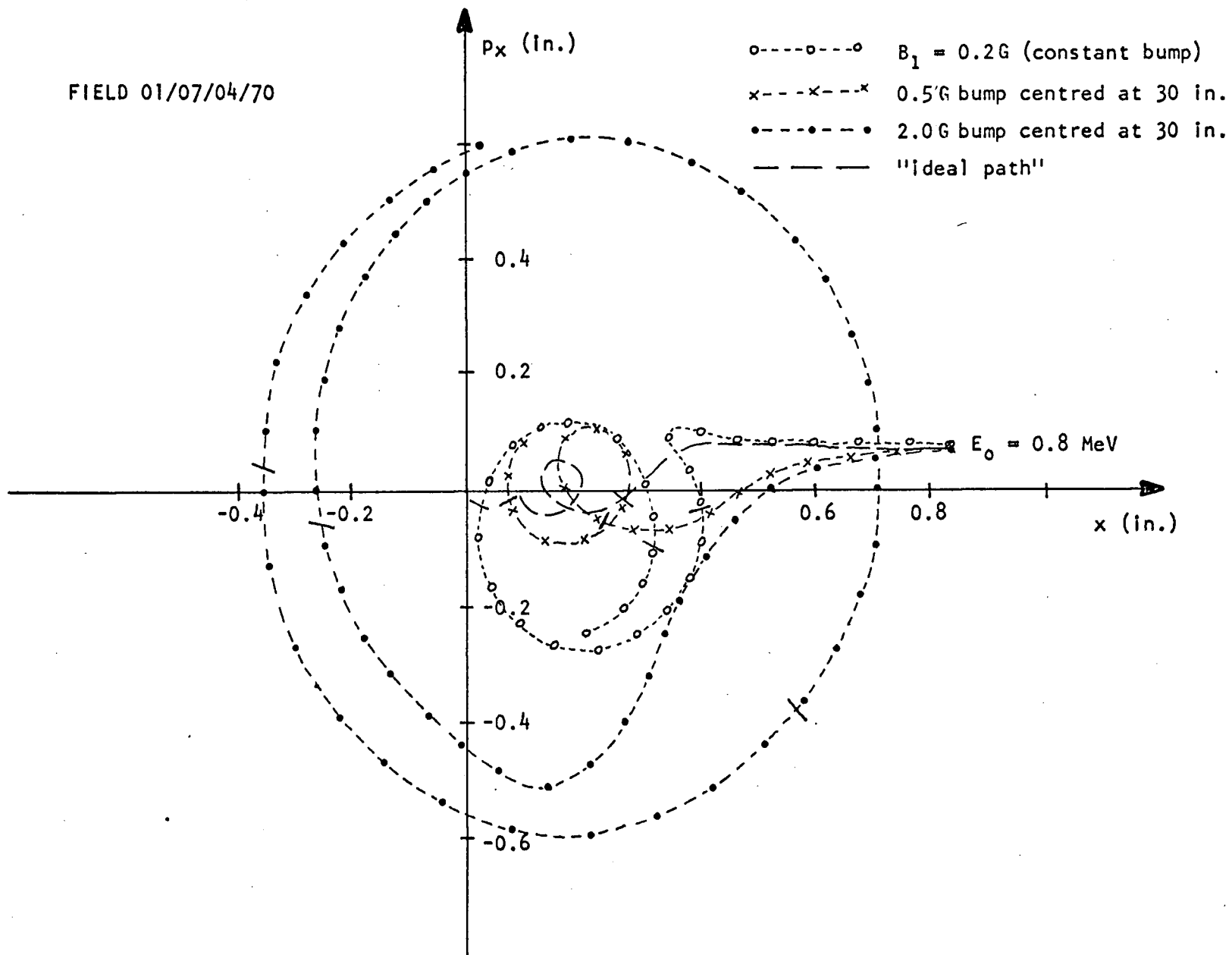


Fig. 3.1. Phase space for accelerated ions (0.8 MeV to 28 MeV) of 0 deg RF phase with various first harmonics present. The markers (/) indicate 5 MeV step.

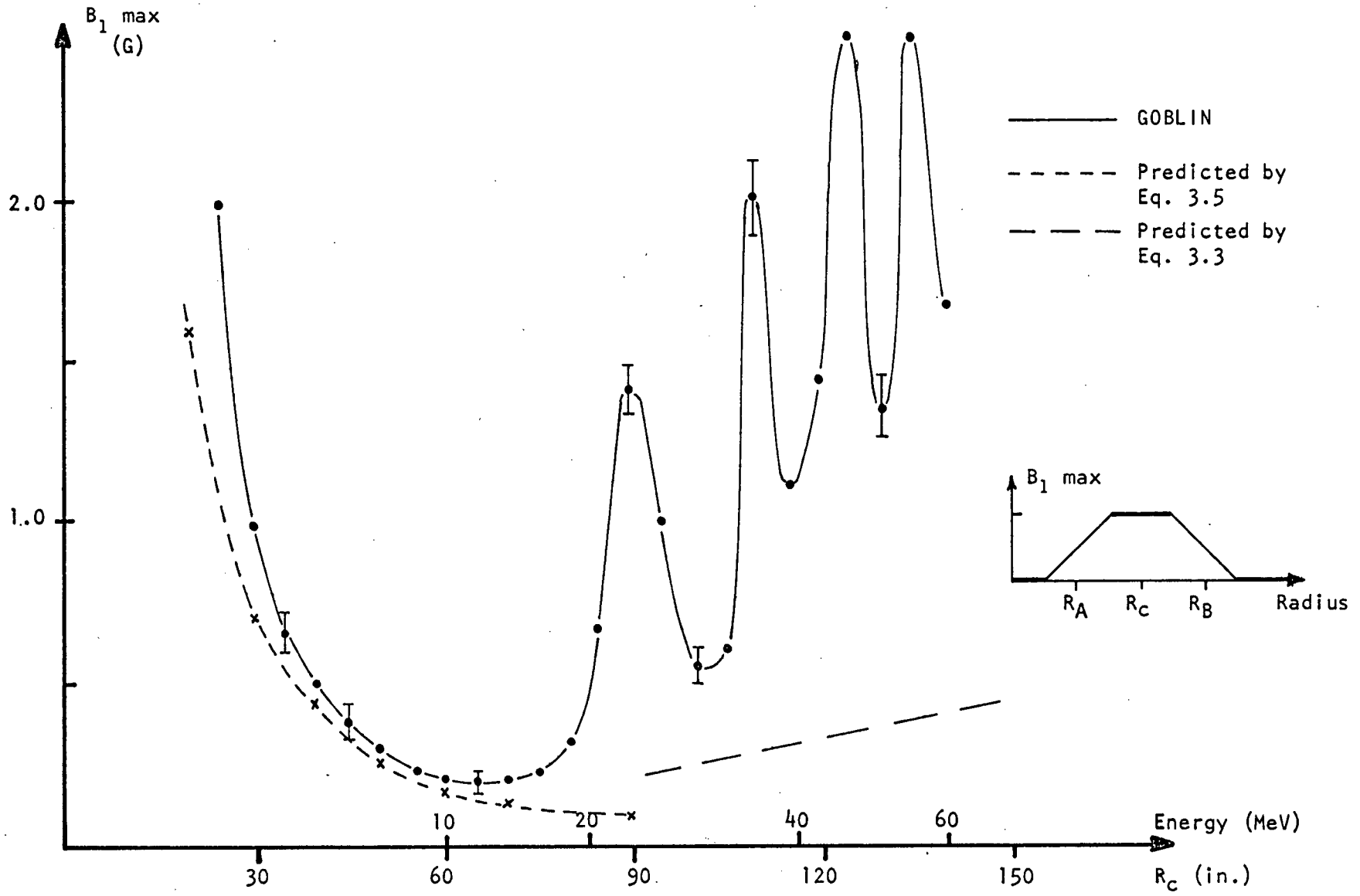


Fig. 3.2. The amplitude of a 20 in. wide ($R_B - R_A$) first harmonic bump required to produce radial betatron amplitudes of 0.2 in.

sensitivity to a first harmonic bump is explained by the fact that the ions only make 4 or 5 turns over the first 30 in. When v_x increases, the oscillatory behaviour of Fig. 3.2 can be explained by the ions making an integral number m or $(m + 1/2)$ complete precession cycles in the bump. A pessimistic assumption would be for the ions to make $(m + 1/2)$ cycles in a "square" bump; in this case, the amplitude acquired would be twice the displacement given in Eq. 3.3. The tolerance on the first harmonic bump is, in that case, tightest, and we obtain a minimum point on the figure. This assumption is, however, pessimistic because, for real bumps with "rounded corners", the particles tend to "follow" the displaced equilibrium orbit when v_x is large. The prediction of this pessimistic assumption and of Eq. 3.5 are shown by the dashed lines in Fig. 3.2.

In practice, the cyclotron field will be shimmed to give a first harmonic of less than 1 G. Then, several sets of six harmonic coils, each extending over 60 deg in azimuth, will be used to compensate for the effect of the remaining amplitude. The effect of these harmonic coils is considered in the next section.

3.3 Harmonic Coils

3.3.1 Oscillatory First Harmonic

A change in the current of any harmonic coil affects the configuration of the magnetic field in the region where the coil is present. The field contribution from any set of harmonic coils will be used chiefly to cancel the first harmonic error field in their vicinity. Fig. 3.3 shows, however, that the harmonic coils may not be able to cancel this intrinsic first harmonic at every point. The amplitude of the residual first harmonic as a function of radius will tend to oscillate between positive and negative values, i.e. its azimuth shifts by 180 deg. We assume a

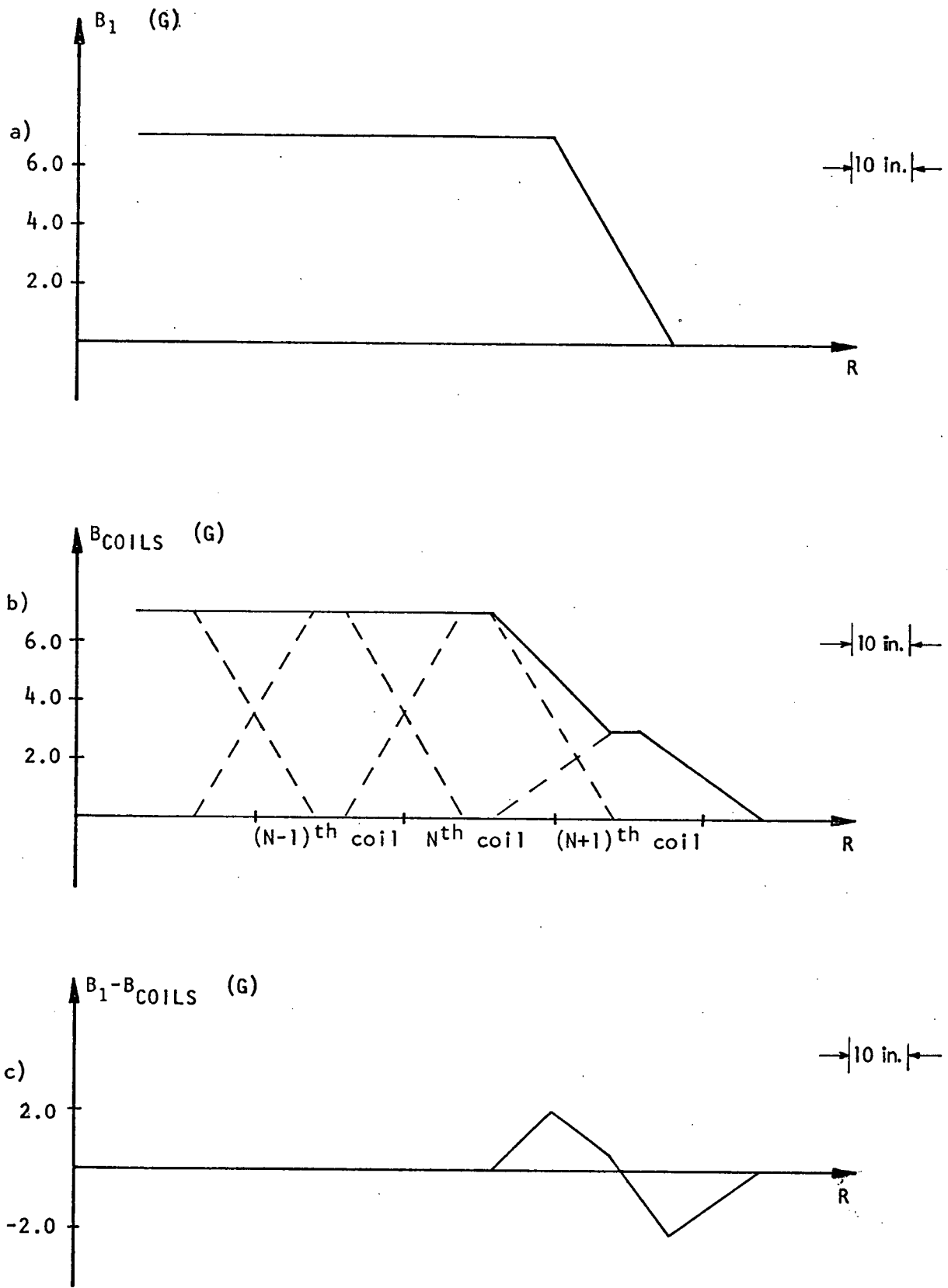


Fig. 3.3. a) First harmonic error field
b) Net coil field corrections
c) Residual first harmonic

purely sinusoidal azimuthal dependence for the coil fields.

As a "bad" case, we chose to consider an intrinsic first harmonic that varied radially in such a way that it was always out of step with the correcting field produced by the coils, i.e. the error is always zero at a coil centre and an extremum half way between their centres. This is not a likely situation. The residual first harmonic is shown in Fig. 3.4; the azimuth is constant with radius (apart from switches of ± 180 deg). The betatron amplitudes resulting from various amplitudes of this oscillatory first harmonic (for ions of 0 deg RF starting phase) are given in Table 3.1; they are similar to those from a flat first harmonic.

Energy (MeV)	Oscillating Bump Amplitude (gauss)		
	0.1	0.2	0.5
35	0.12 in.	0.23 in.	0.57 in.
50	0.10 in.	0.18 in.	0.46 in.

Table 3.1. Betatron amplitudes for 0 deg RF phase ions

It is possible, as we will see, to cancel the final betatron amplitudes at some energy for ions of any given RF phase, by a suitable choice of an additional harmonic coil field. We chose to look at the set of coils extending from 63 in. to 89 in. in radius, and we assumed that they produced the bump profile shown in Fig. 3.5. We accelerated ions from a low energy to 35 MeV at a radius of approximately 107 in. At that energy, the ions are outside the region of sensitivity to a first harmonic and, if centred there, should remain centred during further acceleration. Their end points in (x, p_x) space are given in Fig. 3.6 as functions of the bump

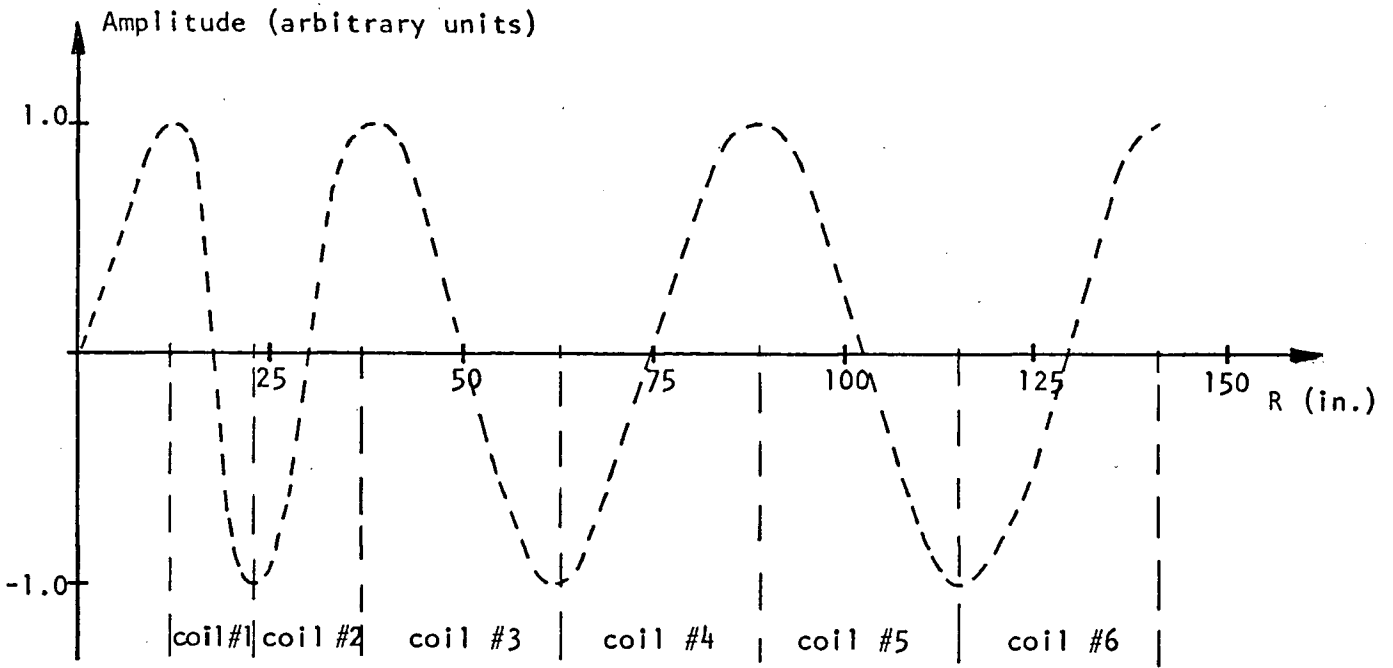


Fig. 3.4. Profile of oscillatory first harmonic

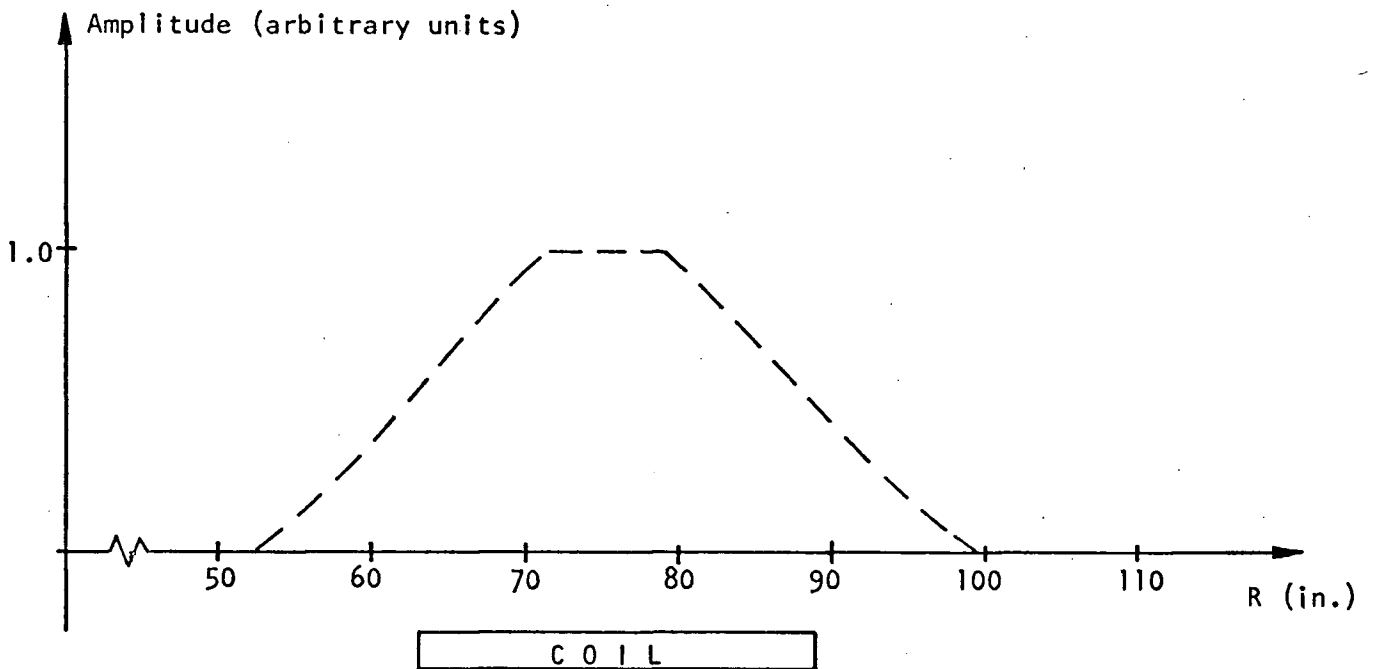
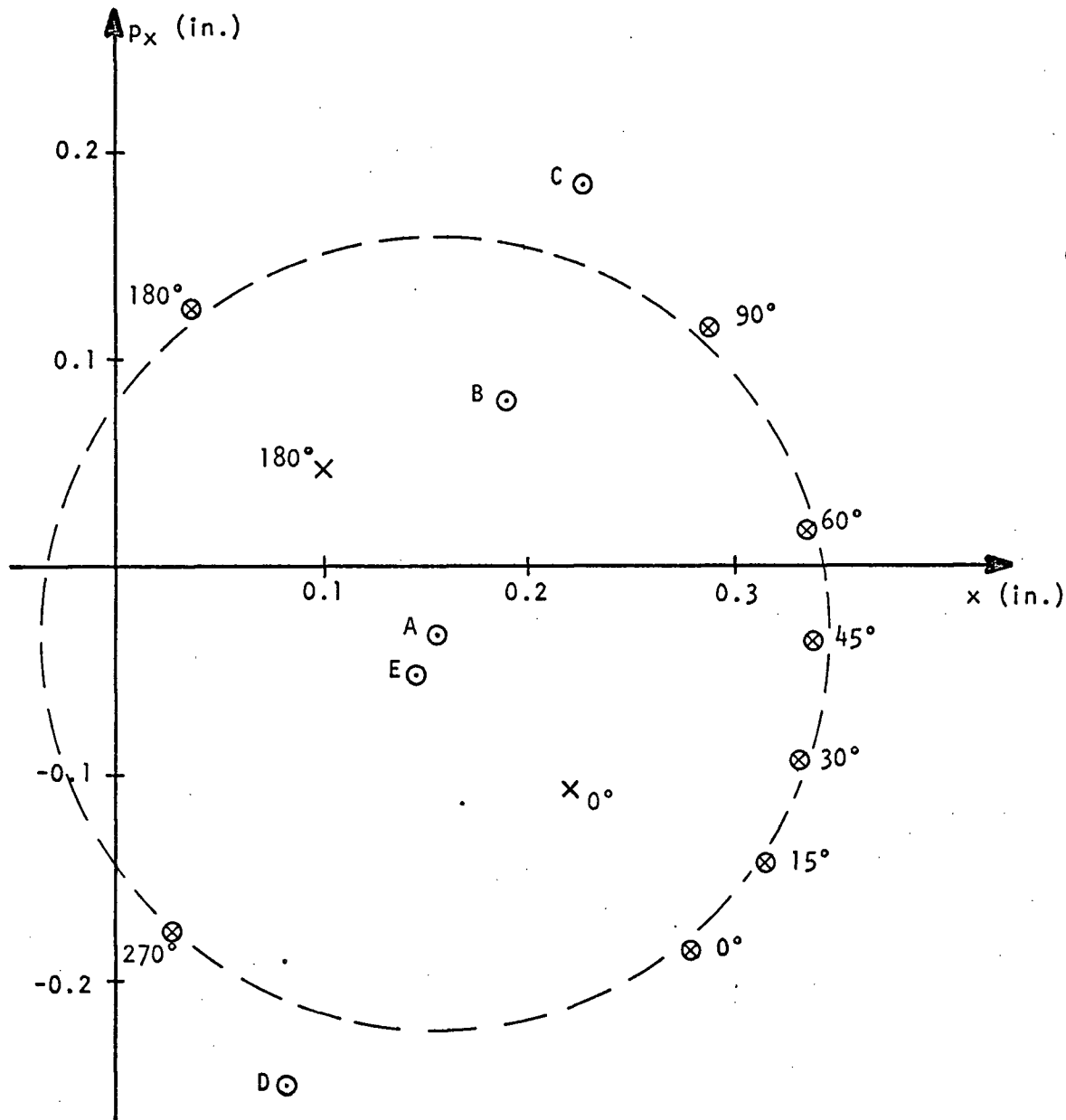


Fig. 3.5. Bump Profile



- X Bump of Fig. 3.5 - Amplitude 0.2 G
- ⊗ Bump of Fig. 3.5 - Amplitude 0.4 G (angle denotes bump azimuth)
- ⊙ A - No imperfection harmonics (ideal case)
- B - Oscillatory first harmonic of 0.1 G
- C - Oscillatory first harmonic of 0.2 G
- D - Point used to estimate bump azimuth and amplitude to cancel C
- E - Result for C + D

Fig. 3.6. Positions at 35 MeV for ions of 0 deg RF phase accelerated from low energy

amplitude and azimuth. The amplitude and azimuth of the displacement are almost linear functions of the amplitude and azimuth of the first harmonic bump.

The end point in the ideal case, when no imperfection harmonics are present, is shown as point A. The end point C for an oscillatory residual field of 0.2 G is also shown; we attempted to cancel this for ions of 0 deg RF phase by an additional bump between 63 in. and 89 in. of 0.47 G at 295 deg. Point D, obtained by drawing a line from C through A and setting AD = AC, was used to estimate this bump amplitude to cancel C. The net result is to bring the ions back to point E. The improvement can be seen by comparing the results in the first column of Table 3.2 with those in Table 3.1 for 0.2 G.

Energy (MeV)	Ion Phase		
	0 deg	15 deg	30 deg
35	0.02 in.	0.03 in.	0.19 in.
50	0.07 in.	0.08 in.	0.12 in.

Table 3.2. Betatron amplitudes with harmonic coil field

Ions that start at the same point and the same energy but different RF phase will acquire different betatron amplitudes primarily because they make more turns to reach a given energy. Their betatron amplitudes will not be cancelled exactly by this bump. To investigate the first harmonic effect alone, it was necessary to remove the "phase-centre point spread" phenomenon.⁸ This was done by running GOBLIN backward to find "ideal"

starting points for different phases; these starting points were displaced from the 0 deg starting point by 0.1 in. for 15 deg and 0.46 in. for 30 deg RF phase. Ions starting at these positions were accelerated through the 0.2 G oscillatory field with the correcting bump, and the results are given in Table 3.2. The final amplitudes for ions at 15 deg are quite acceptable, and those for ions at 30 deg are acceptable for many purposes.

3.3.2 Ions with a Wide Range of RF Phases

In cases where the harmonic coils cannot cancel the first harmonic error field in the magnet, we would like to know if we can choose coil settings that will reduce the betatron amplitudes acquired to a small value at some energy for ions with a wide range of RF phases. The previous section showed that we could do this for a narrow phase width by suitably powering a single coil set.

On Fig. 3.7 we denote as E and β the amplitude and phase of the betatron oscillation induced by the first harmonic error. Similarly, $\vec{\Gamma}$, with amplitude γ and phase ω , represents the oscillation produced by a 1 G field in a single harmonic coil placed at a standard azimuth and is called the coil coefficient. Then, for each set of coils, each RF phase and a given energy, we have

$$\vec{E} = A\vec{\Gamma} \quad (3.7)$$

where A is a complex number with amplitude A (gauss) equal to the coil field required for compensation of the error, and phase α equal to the azimuthal rotation required for the single harmonic coil set considered. In practice, each coil set consists of six coils at 60 deg azimuth intervals and their relative currents can be arranged⁹ to provide a first harmonic peak at the desired azimuth. When several coil sets are used to cancel \vec{E} ,

their effects can be superposed so that Eq. 3.7 becomes

$$\vec{E} = A_1 \vec{I}_1 + A_2 \vec{I}_2 + A_3 \vec{I}_3 + \dots \quad (3.8)$$

We separate real and imaginary parts of Eq. 3.8 and obtain

$$E \cos \beta = (\gamma_1 \cos \omega_1 A_1 \cos \alpha_1 - \gamma_1 \sin \omega_1 A_1 \sin \alpha_1) + (\quad)_2 + (\quad)_3 + \dots \quad (3.9)$$

$$E \sin \beta = (\gamma_1 \sin \omega_1 A_1 \cos \alpha_1 + \gamma_1 \cos \omega_1 A_1 \sin \alpha_1) + (\quad)_2 + (\quad)_3 + \dots \quad (3.10)$$

Then, to keep the equations linear, we rewrite Eq. 3.9 and Eq. 3.10 as

$$E_x = (\gamma_x A_x - \gamma_y A_y)_1 + (\quad)_2 + (\quad)_3 + \dots \quad (3.11)$$

$$E_y = (\gamma_y A_x + \gamma_x A_y)_1 + (\quad)_2 + (\quad)_3 + \dots \quad (3.12)$$

The values of E_x and E_y , at a given energy, are found by superposing the first harmonic error on our magnetic field and measuring the ending point in (x, p_x) space of an ion accelerated to that energy. The coil coefficients are obtained in the same way, using a field of known amplitude in each coil. We then solve a set of linear equations to find A_{1x} , A_{1y} , A_{2x} ,, the amplitudes and phases of the coil correcting fields.

As a very pessimistic case, we chose to cancel the first harmonic error shown on Fig. 3.8. The bump has a 2 G amplitude and extends from 35 in. to 90 in. This region, as we saw previously, is the most sensitive to field imperfections. The three sets of coils at $37'' \leq R \leq 54''$, $54'' < R < 71''$, $71'' < R < 89''$, respectively, can be used to compensate for the effect of the first harmonic imperfection. However, the variation with radius of the first harmonic error was chosen so that the coils could not eliminate it completely. With six coil constants, A_{1x} , A_{1y} ,, A_{3y} , open to choice, it appears possible to satisfy Eq. 3.11 and Eq. 3.12

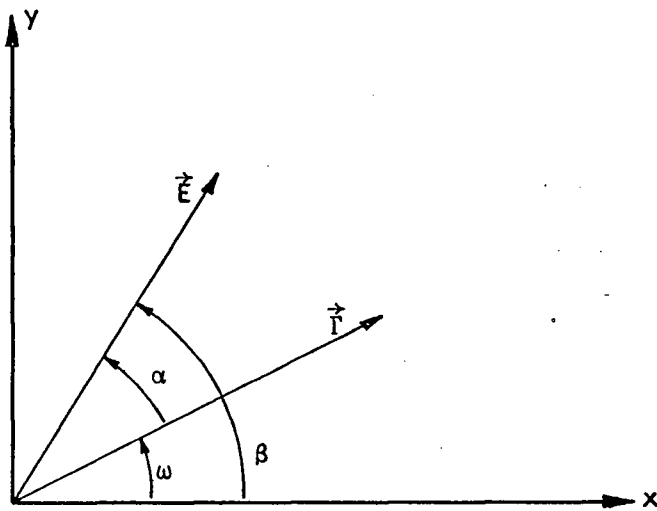


Fig. 3.7. Phases and amplitudes of the oscillations produced by standard harmonic coil field and by first harmonic error

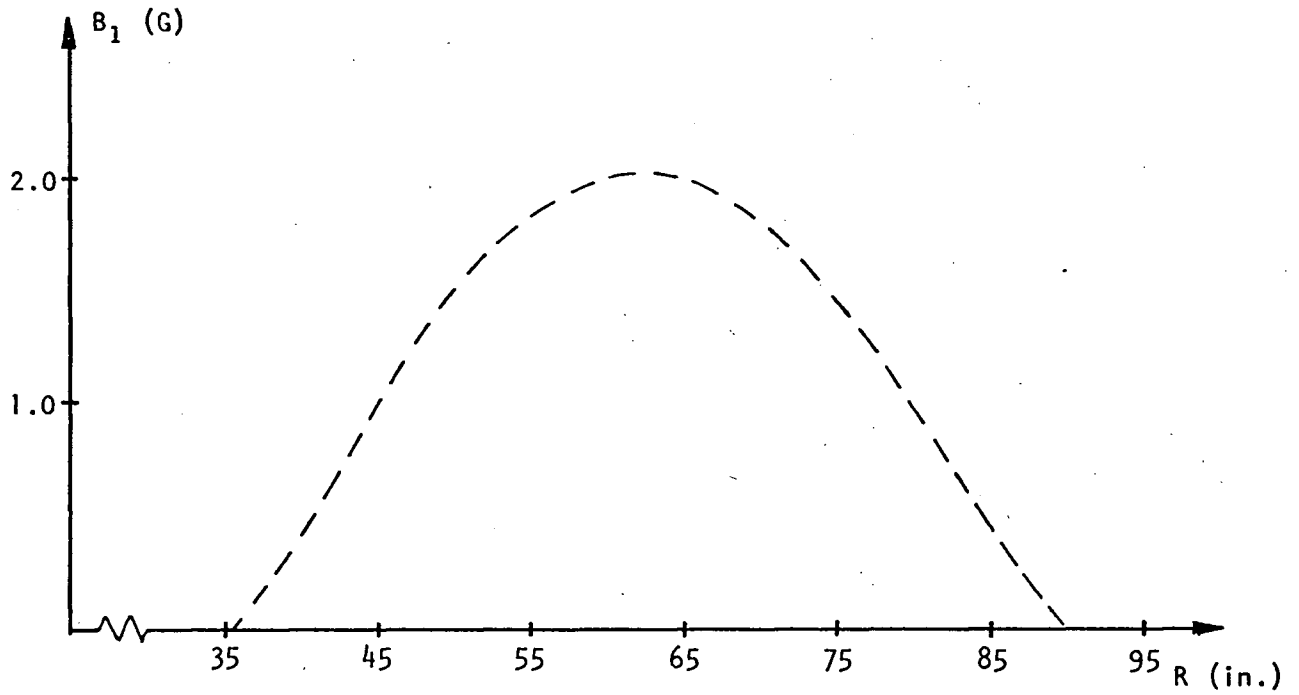


Fig. 3.8. Profile of first harmonic error

simultaneously for ions with three different RF phases. We chose to consider ions with 0 deg, 25 deg, and 40 deg RF phase and tried to centre them at 35 MeV, i.e. approximately 105 in.

All calculations were done using the field 01/30/10/70. We first determined ideal starting conditions for our three particles. Their paths in phase space to 35 MeV are called "ideal paths". We then superposed the first harmonic error and found the ending point of each ion at 35 MeV. Each displacement was measured from the "ideal" centre point at 35 MeV.

Similarly, we obtain the values for the coil coefficients, Γ , by adding a 2 G field in each coil and measuring the corresponding displacement, as shown in Fig. 3.9. We verified that the amplitude of the displacement was proportional to the field amplitude so that the Γ are constant over the range of amplitudes we were using. We also checked that the displacement due to two different coils is the vector sum of the displacements due to each of these two coils.

Once we obtained our set of six linear equations, we found that a small change in the known parameters was giving rise to large changes in the solutions. This phenomenon is known as ill-conditioning. Since we cannot measure betatron amplitudes exactly using probes, we need a less sensitive approach. We therefore measured the displacements due to the first harmonic error at every 5 MeV step from 15 MeV to 35 MeV, and calculated the corresponding values of γ_x and γ_y at those energies. We could also have improved the situation by running additional phases to 35 MeV; however, we chose to get the coefficients at different energies to reduce the number of GOBLIN runs. The results at 5 MeV steps are given in the following tables.

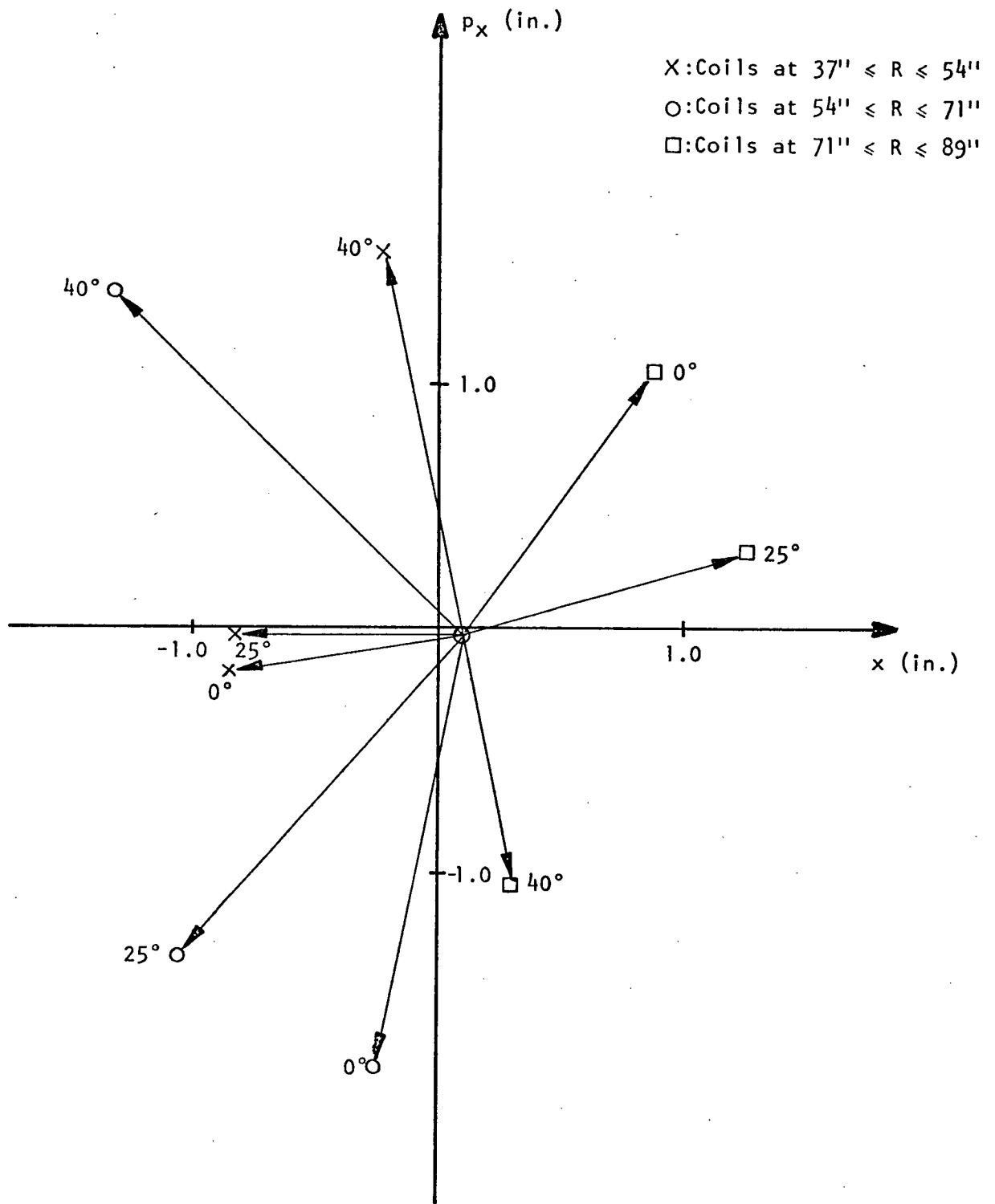


Fig. 3.9. Displacements from "ideal" centre point at 35 MeV due to a 2 G field in each set of coils, for ions of 0° , 25° and 40° RF phase

RF Phase (deg)	Energy (MeV)	15	20	25	30	35
0	E_x (in.)	-1.99	-0.10	0.54	-0.76	-0.10
	E_y (in.)	-0.48	1.84	-1.54	1.43	-1.70
25	E_x (in.)	-2.03	-0.36	0.76	-0.38	-1.00
	E_y (in.)	-0.92	2.22	-1.82	1.99	-1.70
40	E_x (in.)	-2.30	0.45	-0.66	1.34	-1.68
	E_y (in.)	-1.08	2.46	-2.25	1.74	1.17

Table 3.3. Components of displacements due to first harmonic of Fig. 3.8

RF Phase (deg)	Energy (MeV)	15	20	25	30	35
0	γ_x (in./G)	-0.35	0.49	-0.42	0.37	-0.48
	γ_y (in./G)	0.41	0.09	-0.31	0.39	-0.08
25	γ_x (in./G)	-0.46	0.38	-0.25	0.34	-0.48
	γ_y (in./G)	0.17	0.37	-0.50	0.42	0.00
40	γ_x (in./G)	-0.61	0.50	-0.50	0.63	-0.14
	γ_y (in./G)	-0.03	0.46	-0.47	0.01	0.74

Table 3.4. Coefficients for set of coils at $37'' \leq R \leq 54''$

RF Phase (deg)	Energy (MeV)	15	20	25	30	35
0	γ_x (in./G)	-0.73	0.12	0.17	-0.30	-0.17
	γ_y (in./G)	-0.32	0.88	-0.87	0.83	-0.89
25	γ_x (in./G)	-0.72	0.06	0.20	-0.01	-0.60
	γ_y (in./G)	-0.42	0.96	-0.93	0.97	-0.67
40	γ_x (in./G)	-0.79	0.41	-0.43	0.70	-0.69
	γ_y (in./G)	-0.43	0.96	-0.95	0.67	0.66

Table 3.5. Coefficients for set of coils at $54'' \leq R \leq 71''$

RF Phase (deg)	Energy (MeV)	15	20	25	30	35
0	γ_x (in./G)	-0.06	-0.77	0.14	-0.07	0.38
	γ_y (in./G)	-0.18	-0.26	0.70	-0.69	0.54
25	γ_x (in./G)	-0.06	-0.77	0.15	-0.29	0.56
	γ_y (in./G)	-0.19	-0.28	0.70	-0.60	0.17
40	γ_x (in./G)	-0.07	-0.83	0.35	-0.47	0.12
	γ_y (in./G)	-0.21	-0.11	0.40	-0.01	-0.55

Table 3.6. Coefficients for set of coils at $71'' \leq R \leq 89''$

We thus obtained a set of 30 linear equations for our six unknowns. A least squares fitting program was written to minimize

$$\sum_{I=1}^{30} W(I) \left(E(I) - \sum_{J=1}^6 A(J) \cdot \gamma(I,J) \right)^2 \quad (3.13)$$

where $W(I)$ is a weighting term. With weights of 0.5, 1, 2, 3, 3 for energies of 15 MeV to 35 MeV, the amplitudes and phases of the harmonic coil fields to cancel the first harmonic error were found to be

	1st coil	2nd coil	3rd coil
A (G)	0.61	2.07	0.75
α (deg)	6.3	4.1	-24.0

Table 3.7. Harmonic coil correcting fields

We determined that the coil requirements were no longer sensitive to input parameters. The solutions $A(J)$ were then used to calculate the displacements from the ideal orbit at energies where the coefficients were calculated, since the $A(J)$'s obtained are the best solution but may not result in absolutely zero final displacement.

The initial displacements from the ideal orbit due to the first harmonic error are given in Table 3.8.

E (MeV) φ RF (deg)	15	20	25	30	35
0	2.05 in.	1.84 in.	1.63 in.	1.62 in.	1.70 in.
25	2.23 in.	2.25 in.	1.97 in.	2.03 in.	1.97 in.
40	2.54 in.	2.50 in.	2.34 in.	2.20 in.	2.05 in.

Table 3.8. Displacements from ideal orbit due to first harmonic of Fig. 3.8

The final displacements, when both the first harmonic error and the correcting fields are present, are given in the following table.

E (MeV) φ RF (deg)	15	20	25	30	35
0	0.26 in.	0.18 in.	0.02 in.	0.07 in.	0.02 in.
25	0.28 in.	0.10 in.	0.04 in.	0.03 in.	0.14 in.
40	0.27 in.	0.11 in.	0.07 in.	0.09 in.	0.14 in.

Table 3.9. Displacements from ideal orbit when first harmonic error and correcting fields are present

We see that the displacements have been reduced everywhere by at least a factor 8 and in most cases by much more. We then ran GOBLIN to look at the

phase space for accelerated particles. The results for ions of 0 deg and 40 deg RF phases are shown in Fig. 3.10 and Fig. 3.11. The final amplitudes can be compared to the amplitudes of the residual oscillations obtained in the "ideal" cases. Also shown in Fig. 3.12 is the result for an ion of 30 deg RF phase. This last figure shows that our solution is also valid for ions with intermediate RF phases. Also, since we have shown the effects of a first harmonic to be linear in our machine, we do not expect any distortion of the emittance from these effects. Our solution does not reduce to zero the amplitude of the final oscillation at 35 MeV. This amplitude depends on the form of the first harmonic error present and could be worse or better for a different shape.

In this analysis we eliminated interference from the "phase-centre point spread" phenomenon⁸ by finding an "ideal" starting point for each phase. However, we have shown that it is possible to use the method described above to centre at a given energy ions with different RF phases and identical starting conditions. The required coil fields are obtained in the same manner as in the case of an intrinsic first harmonic imperfection. In other words, we can reduce the centring error, no matter what the cause.

3.4 Sensitivity to a Second Harmonic

In a previous study, Hagedoorn and Verster¹⁰ described the radial motion of the ion on the basis of the Hamiltonian formalism. The influence of small field errors introduced by first and second harmonic was also considered. They showed that radial instability caused by a second harmonic of amplitude B_2 is present if

$$\frac{B_2}{2B} + \frac{Re_0}{4B} \frac{\partial B_2}{\partial R} \geq \nu_x - 1. \quad (3.14)$$

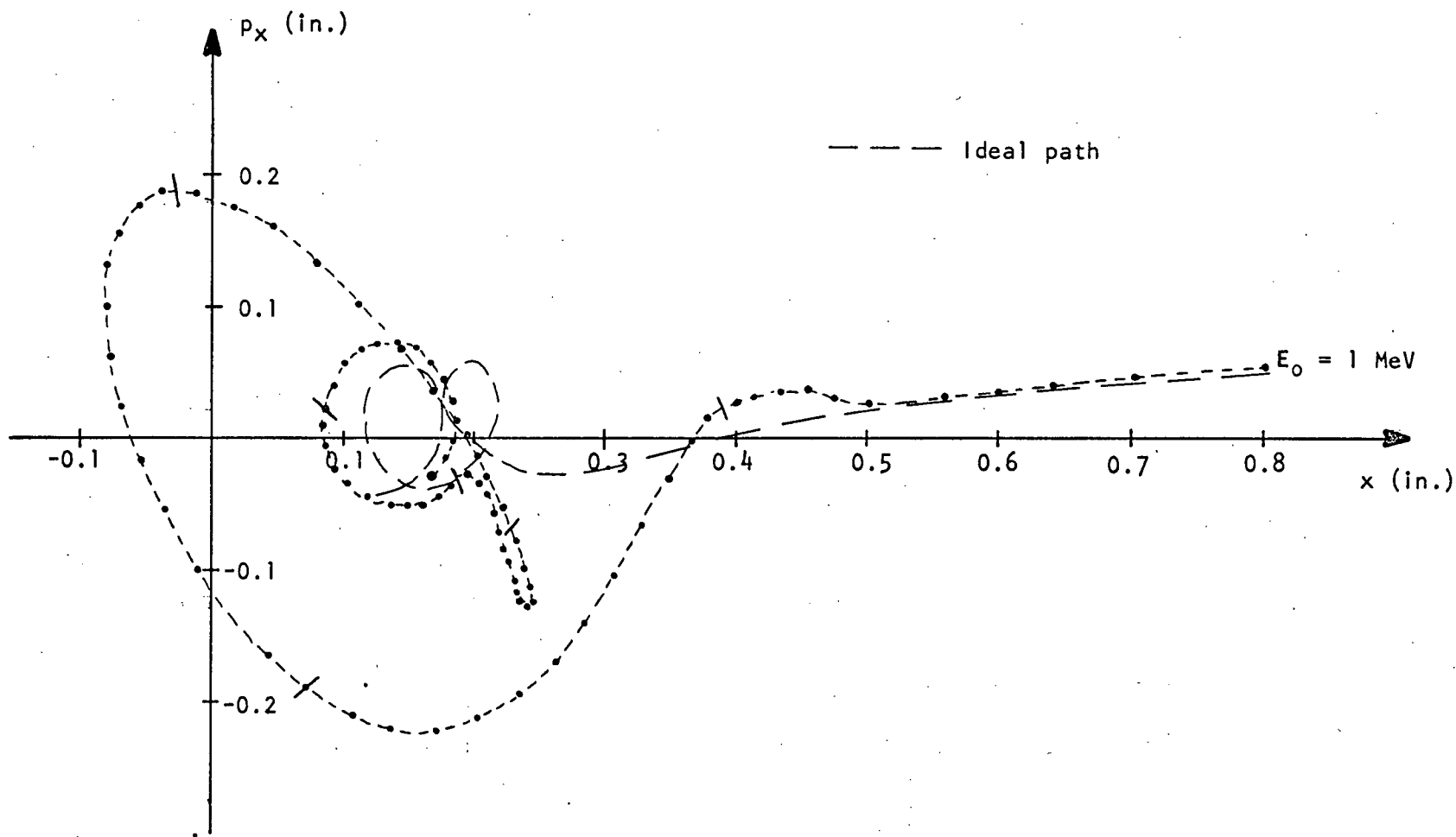


Fig. 3.10. Phase space plot for accelerated ions (1 MeV to 35 MeV) of 0 deg RF phase with both the first harmonic error and the harmonic coil correcting fields present. The markers (/) indicate every 5 MeV step.

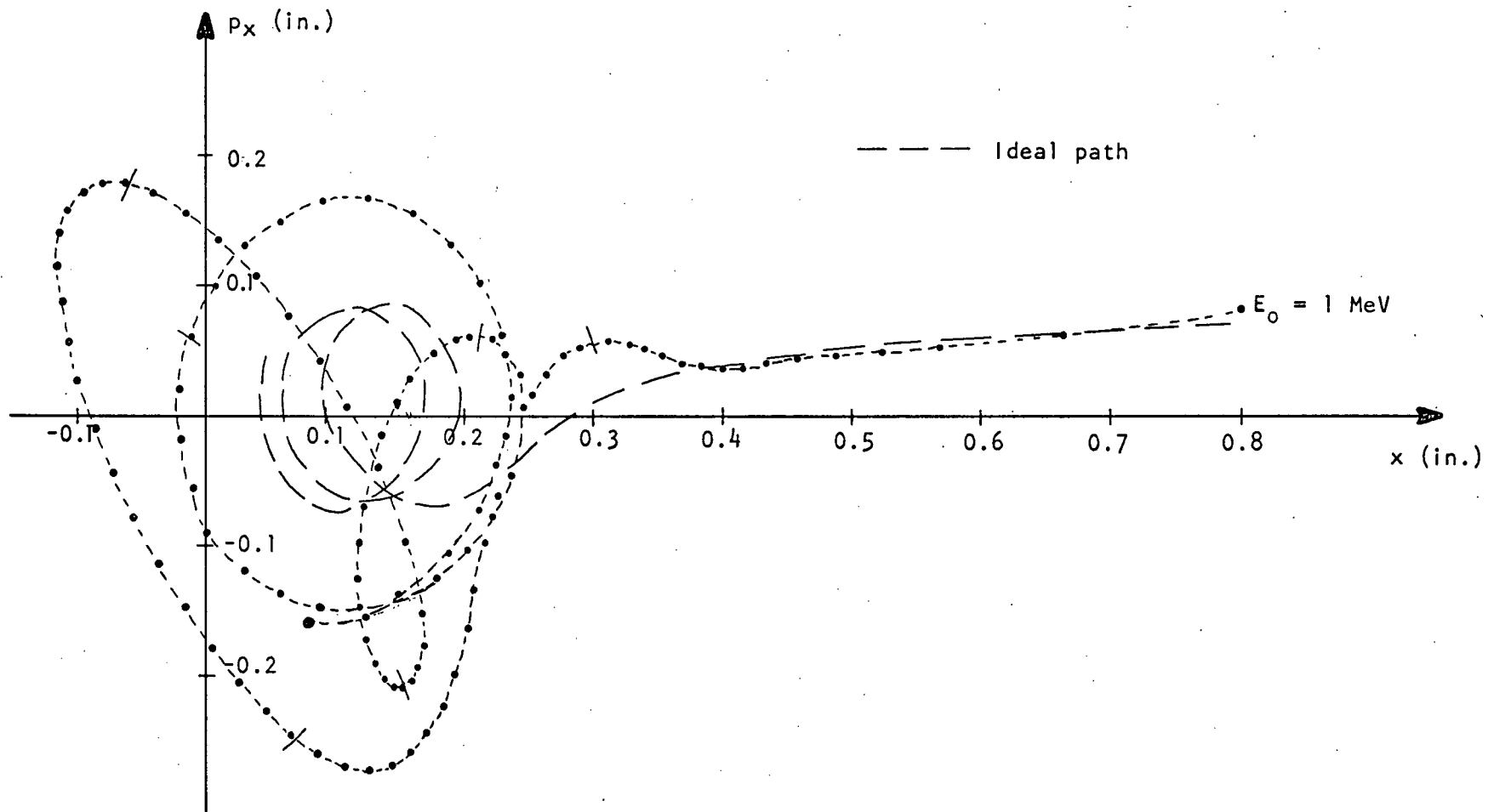


Fig. 3.11. Phase space plot for accelerated ions (1 MeV to 35 MeV) of 40 deg RF phase with both the first harmonic error and the harmonic coil correcting fields present. The markers (/) indicate every 5 MeV step.

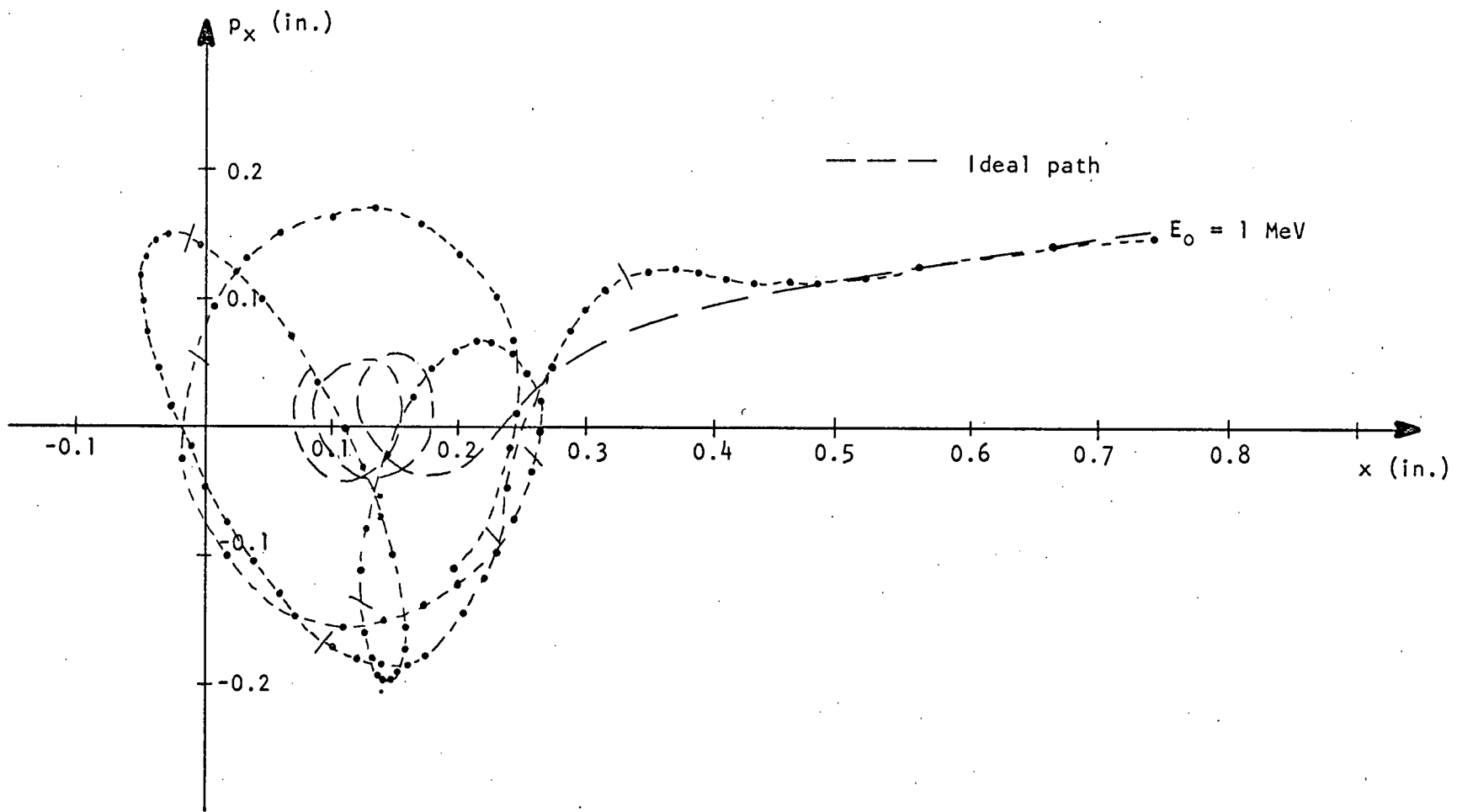


Fig. 3.12. Phase space plot for accelerated ions (1 MeV to 35 MeV) of 30 deg RF phase with both the first harmonic error and the harmonic coil correcting fields present. The markers (//) indicate every 5 MeV step.

On Fig. 3.13 we have plotted the left-hand side of this last expression for various values of v_x , using the field 01/30/06/70. The region on the right-hand side of each line is the instability region for that particular value of v_x . The corresponding values of the amplitude and gradient of the second harmonic will, in these regions, lead to an imaginary value of v_x , i.e. complete defocusing. Using our code CYCLOP to verify Eq. 3.14, we obtained imaginary values of v_x with second harmonics whose amplitudes and gradients were within 20% of the values obtained from Eq. 3.14. Thus, Fig. 3.13 can be considered a useful guide to set our tolerances on the second harmonic. Even if the second harmonic is not sufficient to render v_x imaginary, it can still distort the static phase space ellipse; we consider a reasonable tolerance to be about 1/4 of the critical values given in Fig. 3.13.

Finally, when we considered a mixture of both first and second harmonic errors, we observed that the shift of the equilibrium orbit, at low energy, was strongly dependent on the relative phase of the harmonics. As it stands, Eq. 3.3 does not take into account the phase of the harmonics. However, we can understand this phenomenon with the use of the Hamiltonian derived by Hagedoorn and Verster to describe the motion of the orbit centre.

The contribution of the first and second harmonic to the Hamiltonian may be written

$$H = \frac{x B_1}{R_{e0} B} \cos(\theta - \phi_1) + \frac{x^2}{2 R_{e0}^2} \left((v_x - 1) + \frac{B_2}{2B} \cos(2\theta - \phi_2) \right) \quad (3.15)$$

where x is the displacement from the equilibrium orbit radius R_{e0} , and ϕ_1 and ϕ_2 are the phases of the two harmonics. For greater simplicity, Eq. 3.15 has been written without the terms involving the gradients of the

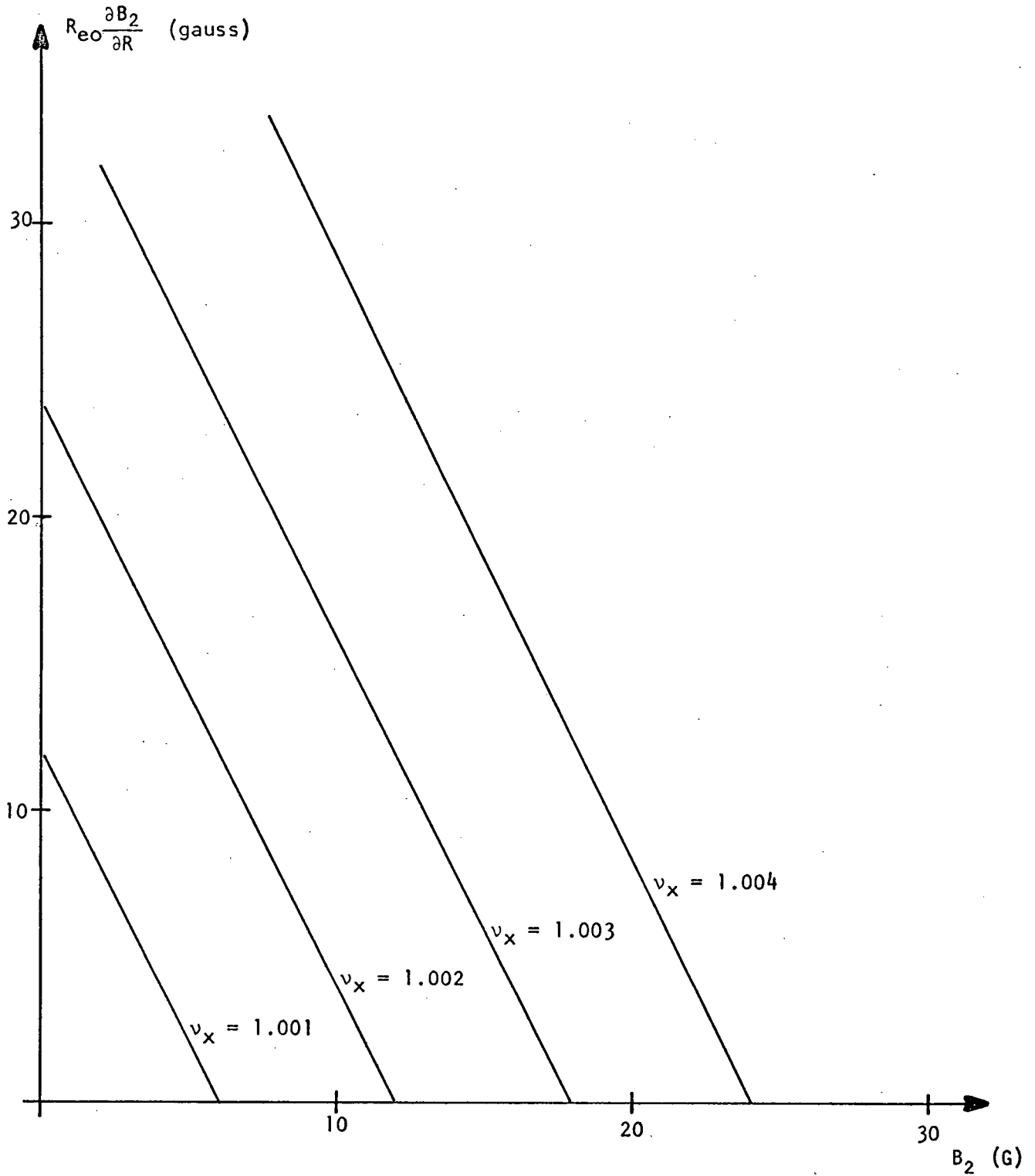


Fig. 3.13. Limits of radial stability for second harmonic error field

of the harmonics. The new position of the orbit centre follows from

$\frac{\partial H}{\partial x} = 0$. We obtain

$$x \approx \frac{B_1 R_{eo}}{2B(\nu_x - 1)} \cos(\theta - \phi_1) - \frac{B_1 B_2 R_{eo}}{4B^2(\nu_x - 1)^2} \cos(\theta - \phi_1) \cos(2\theta - \phi_2) + \dots (3.16)$$

Since $(\nu_x^2 - 1) \approx 2(\nu_x - 1)$, we verify that Eq. 3.3 and Eq. 3.16 are equivalent when no second harmonic is present.

Table 3.10 and Table 3.11 show the displacements obtained from numerical estimates using CYCLOP and from Eq. 3.16 for ions of 1 MeV and 3 MeV.

Phases of Imperfection Harmonics	$\phi_1 = \phi_2 = 0$ deg	$\phi_1 = 0$ deg $\phi_2 = 90$ deg	$\phi_1 = 90$ deg $\phi_2 = 0$ deg	$\phi_1 = \phi_2 = 90$ deg
CYCLOP	1.98 in.	3.04 in.	4.02 in.	2.93 in.
Eq. 3.16	2.08 in.	3.12 in.	4.16 in.	3.12 in.

Table 3.10. Displacements of the equilibrium orbit centre due to first and second imperfection harmonics of 1 G and 2 G, respectively, for ions of 0 deg RF phase at 1 MeV and $\nu_x = 1.001$

Phases of Imperfection Harmonics	$\phi_1 = \phi_2 = 0$ deg	$\phi_1 = 0$ deg $\phi_2 = 90$ deg	$\phi_1 = 90$ deg $\phi_2 = 0$ deg	$\phi_1 = \phi_2 = 90$ deg
CYCLOP	1.11 in.	1.22 in.	1.33 in.	1.23 in.
Eq. 3.16	1.24 in.	1.35 in.	1.46 in.	1.35 in.

Table 3.11. Displacements of the equilibrium orbit centre due to first and second imperfection harmonics of 1 G and 2 G, respectively, for ions of 0 deg RF phase at 3 MeV and $\nu_x = 1.004$

We assumed a maximum value for the displacement, and the amplitudes of the first and second harmonic were of 1 G and 2 G, respectively.

The displacement of the equilibrium orbit centre is a minimum when both harmonics are in phase at 0 deg. In the cases where $\phi_1 = 0$ deg, $\phi_2 = 90$ deg or $\phi_1 = \phi_2 = 90$ deg, the second term on the left-hand side of Eq. 3.16 goes to zero so that the displacement of the equilibrium orbit centre is due only to the first harmonic error. In all the cases we considered, the accuracy of Eq. 3.16 was within 10%, for small values of $(v_x - 1)$. Because this shift decreases rapidly with the increasing energy and also because the ion spends just a few turns in the central region, the displacements can be tolerated.

4. THE RESONANCE $\nu_x - \nu_z = 1$

4.1 Mathematical Description

The second order linear coupled resonance $\nu_x - \nu_z = 1$ will be encountered at about 150 MeV, with $\nu_x \approx 1.2$ and $\nu_z \approx 0.2$. This resonance, like others involving an odd multiple of ν_z , is driven by an asymmetry in the median plane of the cyclotron. For example, the asymmetry may be caused by a tilt of the magnet sectors. Only the first harmonic of such a tilt or twist is of importance in driving this resonance.

To describe the effect of this resonance, we reproduce a portion of the analysis due to Joho.¹¹ He assumes a Hamiltonian of the form $H = H_0 + H_1$ where

$$H_0 = \frac{1}{2} \left(\nu_x^2 x^2 + p_x^2 \right) + \frac{1}{2} \left(\nu_z^2 z^2 + p_z^2 \right) = \text{harmonic oscillator term} \quad (4.1)$$

$$H_1 = a x z \cos(\theta - \theta_0) = \text{coupling term} \quad (4.2)$$

He then constructs a sequence of canonical transformations which eliminate the θ -dependent parts of the Hamiltonian. The first transformation introduces the so-called action-angle variables. In terms of these variables $(\phi_x, J_x, \phi_z, J_z)$, the old variables are given by

$$x = \sqrt{\frac{2J_x}{\nu_x}} \cos(\phi_x - \nu_{x0}\theta) \quad (4.3)$$

$$p_x = \sqrt{2\nu_x J_x} \sin(\phi_x - \nu_{x0}\theta)$$

$$z = \sqrt{\frac{2J_z}{\nu_z}} \cos(\phi_z - \nu_z\theta)$$

$$p_z = \sqrt{2\nu_z J_z} \sin(\phi_z - \nu_z\theta)$$

where ν_{x0} is a reference frequency such that $\Delta\nu \equiv \nu_x - \nu_z - 1 = \nu_x - \nu_{x0} = 0$

when we are exactly on the resonance. The final Hamiltonian is written

$$H^* = -\Delta v J_x - a \left(\frac{J_x}{2v_x} \right)^{\frac{1}{2}} \left(\frac{J_z}{2v_z} \right)^{\frac{1}{2}} \cos(\phi_x - \phi_z - \theta_0). \quad (4.4)$$

This Hamiltonian is independent of θ and is therefore a constant of the motion. If the curves $H^* = \text{constant}$ in phase space are closed, the motion must be stable; otherwise, instability may occur. Joho has shown that, in the case of the difference resonance $v_x - v_z = 1$ the curves in (x_0, z_0) space are given by

$$J_0 = \frac{1}{2} \left(v_x x_0^2 + v_z z_0^2 \right) = \text{constant} \quad (4.5)$$

where J_0 is the total "energy" of the system and x_0, z_0 are the instantaneous amplitudes of the oscillations in units of the average radius, and are determined by the initial conditions. Eq. 4.5 represents an ellipse in (x_0, z_0) space; the motion is periodic and therefore stable, if one amplitude increases, the other decreases. There is effective transfer of energy between the two motions. The total amplitude increase depends, of course, on J_0 , the total available energy.

The next step is to obtain the expressions for the maximum amplitude increases per turn. We first write the Hamiltonian in terms of the normalized action variable ρ_x and the auxiliary variable ρ_z where

$$\rho_x \equiv \frac{J_x}{|J_0|} = \frac{v_x}{2|J_0|} x_0^2 \quad (4.6)$$

$$\rho_z \equiv \frac{J_z}{|J_0|} = \frac{v_z}{2|J_0|} z_0^2 = 1 - \rho_x. \quad (4.7)$$

The Hamiltonian becomes

$$K(\rho_x, \Phi) = -\Delta v \rho_x - \kappa \rho_x^{\frac{1}{2}} \rho_z^{\frac{1}{2}} \cos \Phi \quad (4.8)$$

where $\Phi = \phi_x - \phi_z - \theta_0$ is the relative phase of the two oscillations. The quantity κ is called the "critical frequency" and is given by

$$\kappa = \frac{\alpha_1 (v_x^2 - v_z^2)}{2(v_x v_z)^{\frac{1}{2}}} = \frac{\alpha_1 (v_x + v_z)}{2\sqrt{v_x v_z}} \quad (4.9)$$

where α_1 is the first harmonic of the tilt $\alpha(\theta)$ and is obtained from

$$\alpha_1 = \frac{1}{\pi} \int_0^{2\pi} \alpha(\theta) \cos(\theta - \theta_1) d\theta. \quad (4.10)$$

This critical frequency gives roughly the range of Δv for which the resonance will be excited. The equations of motion follow from $\rho'_x = -\partial K / \partial \Phi$ and $\Phi' = \partial K / \partial \rho_x$, where the prime denotes differentiation with respect to θ . We obtain

$$\rho'_x = -\kappa \rho_x^{\frac{1}{2}} \rho_z^{\frac{1}{2}} \sin \Phi \quad (4.11)$$

$$\Phi' = -\Delta v - \frac{\kappa}{2} \left[(\rho_z / \rho_x)^{\frac{1}{2}} - (\rho_x / \rho_z)^{\frac{1}{2}} \right] \cos \Phi. \quad (4.12)$$

Now, Eq. 4.6 and Eq. 4.7 give

$$\rho'_x / \rho_x = 2 x'_0 / x_0 \quad (4.13)$$

and

$$\rho_z / \rho_x = \frac{v_z z_0^2}{v_x x_0^2} \quad (4.14)$$

so that Eq. 4.11 becomes

$$x'_0 = -\frac{\kappa}{2} \left(\frac{v_z}{v_x} \right)^{\frac{1}{2}} z_0 \sin \Phi. \quad (4.15)$$

The increase in x per turn is given by $2\pi x'_0$ and the maximum occurs when $\sin \Phi = 1$, i.e.

$$\frac{\partial x}{\partial n} \Big|_{\max} = -\pi \kappa \left(\frac{v_z}{v_x} \right)^{\frac{1}{2}} z_0 = -\frac{\pi \alpha_1}{2} \frac{(v_x + v_z)}{v_x} z_0. \quad (4.16)$$

Similarly, the maximum rate of growth for the vertical oscillation is given by

$$\left. \frac{\partial z}{\partial n} \right|_{\max} = \pi K \left(\frac{v_x}{v_z} \right)^{\frac{1}{2}} x_0 = -\frac{\pi \alpha_1}{2} \frac{(v_x + v_z)}{v_z} x_0. \quad (4.17)$$

The above results are only valid in a static situation, i.e. for ions rotating in the resonance region with a fixed energy. Since it is associated with $\Phi = \pi/2$, the maximum amplitude increase will be achieved, for a twist phase of $\theta_0 = 0$ deg, only by those particles with a relative phase of 90 deg. In practice, however, this condition is unlikely to be satisfied by a great number of ions. Moreover, when the particles are accelerated, the frequency shift phenomenon destroys the resonance condition, so that Eq. 4.16 and Eq. 4.17 are really approximate expressions for the maximum rate of growth of the oscillations.

4.2 Calculations

All calculations were done using the field 01/30/10/70 where the resonance occurs at 153 MeV. We simulate a twist in the median plane by assuming, in our GOBLIN code, that two of the magnet sectors, 180 deg apart, are tilted by an angle α . A schematic representation of such a tilted median plane is shown in Fig. 4.1, where R_0 is the radius at which the tilted plane intersects the median plane. In this case, where two sectors are tilted, we have $\alpha_1 \approx \frac{2}{3} \alpha$. The tilt is simulated in the orbit code by rotating the co-ordinate system of the particle each time it enters the region of a tilted sector. The transformation to the new system (R^*, z^*) is written as

$$(R^* - R_0) = (R - R_0) \cos \alpha + z \sin \alpha \quad (4.18)$$

$$z^* = z \cos \alpha - (R - R_0) \sin \alpha + b \quad (4.19)$$

where the constant b is added to simulate the case where the sector is simply lifted by a constant amount. If we assume that α is small, Eq. 4.18 and Eq. 4.19 may be written

$$R^* = R + \alpha z \quad (4.20)$$

$$z^* = z - \alpha(R - R_0) + b. \quad (4.21)$$

Similarly, the particle momenta are changed according to

$$p_R^* = p_R + \alpha p_z \quad (4.22)$$

$$p_z^* = p_z - \alpha p_R. \quad (4.23)$$

The field components, in the region of a tilted sector, are then calculated using the new (R^*, z^*) co-ordinates. When the particle leaves that sector, the reverse transformation is performed.

As an illustration, we chose to consider the case of an ion with an initial phase $\phi_x = 0$ deg for the radial oscillation. From Eq. 4.3, we find that this condition is satisfied, provided the ion is displaced in the positive x -direction. The corresponding condition for the vertical oscillation leading to a maximum rate of growth would be $\phi_z = -\pi/2 - \theta_0$, i.e. a negative p_z displacement if $\theta_0 \approx 0$ deg. These conditions are, however, only true for upright ellipses in phase space. Since, in practice, the ellipses are slanted because of the modulation of the betatron oscillations by the magnet sector structure, we fixed the radial displacement at 0.25 in. and, from the corresponding static (z, p_z) phase space ellipse at 153 MeV, on resonance, we chose eight particles with different starting conditions. The ellipse, obtained with no twisted median plane present, is shown on Fig. 4.2. We then introduced a first harmonic twist, with a slope of $\alpha = 0.02$ rad, about the average radius of the equilibrium orbit

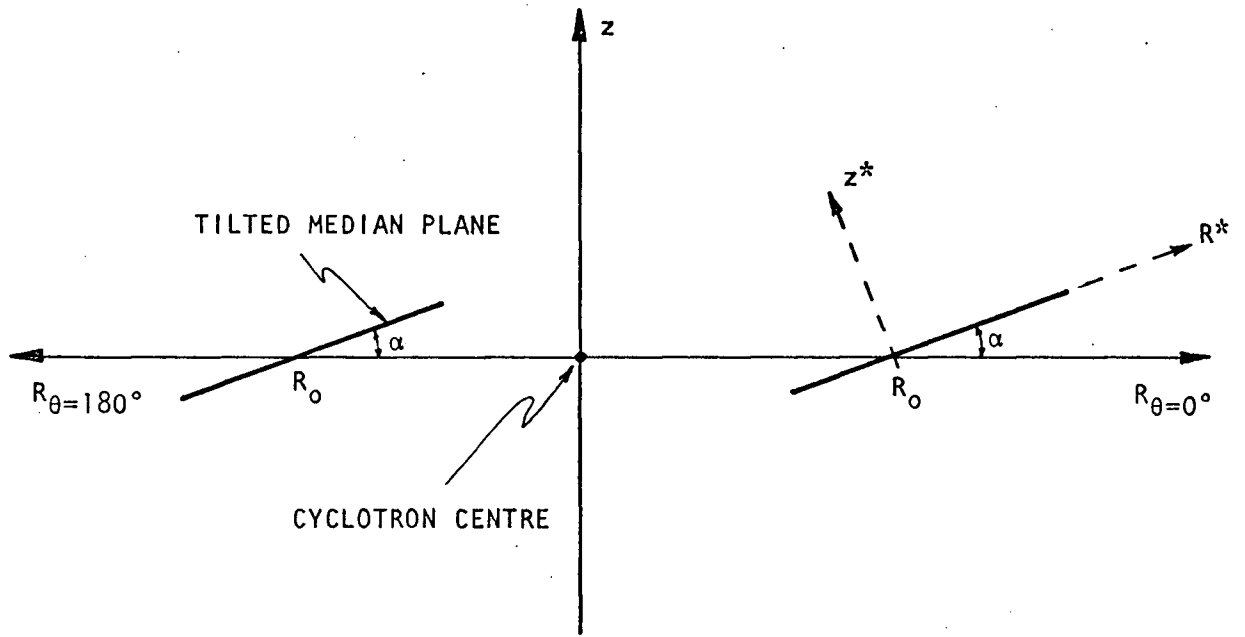


Fig. 4.1. Section view of the cyclotron median plane with tilted median plane parameters

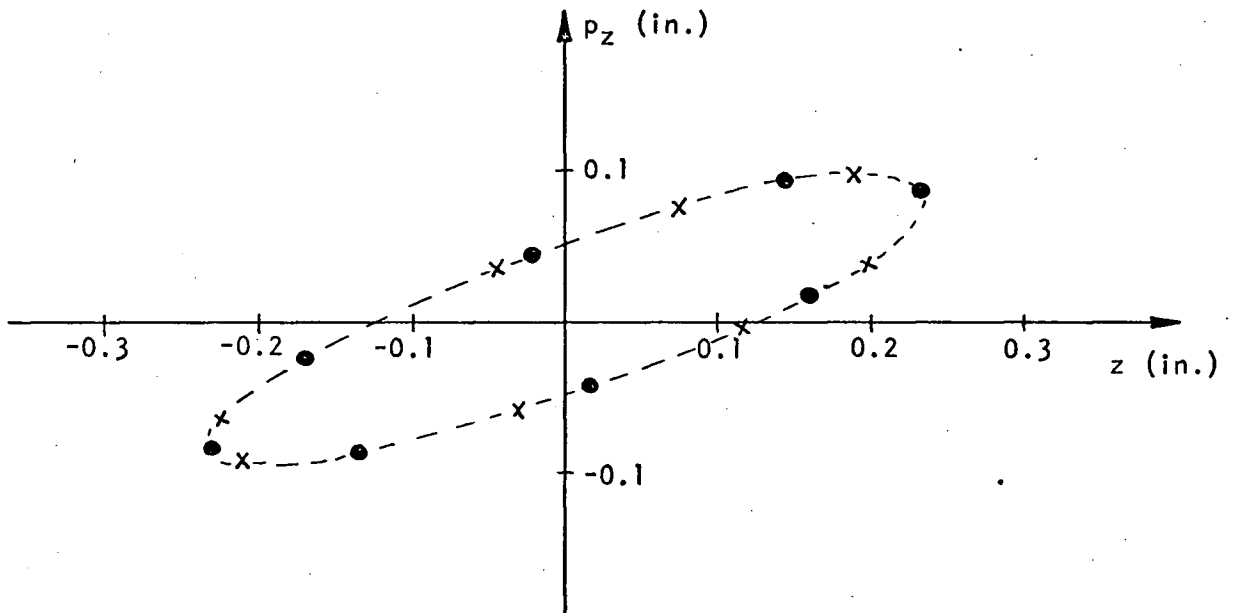


Fig. 4.2. Static phase space ellipse at 153 MeV corresponding to a radial betatron amplitude of 0.25 in. The dots indicate the initial conditions for our eight particles.

at 153 MeV and made static GOBLIN runs at that energy to measure in each case the rate of growth of the oscillations. The particle with initial displacement of $z = 0.145$ in. and $p_z = 0.09$ in. had the maximum rate of growth. As illustrated in Fig. 4.3, the maximum rate of growth is 0.016 in. per turn for the radial oscillation and 0.05 in. per turn in the vertical direction, with a beat period of approximately 40 turns. The minimum amplitude of the radial oscillation is close to zero and the corresponding amplitude in the z-motion is 0.7 in. There is almost complete transfer of energy from the radial to the vertical motion. Eq. 4.5, with initial values of $x_0 = 0.25$ in. and $z_0 = 0.145$ in., gives $J_0 = 0.04 = \text{const.}$; if the amplitude of the radial oscillation decreases to zero, then Eq. 4.5 predicts an amplitude of 0.63 in. for the vertical oscillation. Similarly, we can compare the results obtained for the rate of growth with those predicted by Eq. 4.16 and Eq. 4.17. As seen in Fig. 4.3, the values of x_0 and z_0 at the positions of maximum growth are, respectively, $x_0 = 0.25$ in. and $z_0 = 0.6$ in. so that, with $\alpha_1 \approx \frac{2}{3}\alpha$, Eq. 4.16 gives $|\partial x/\partial n|_{\text{max}} \approx 0.014$ in./turn and Eq. 4.17 gives $|\partial z/\partial n|_{\text{max}} \approx 0.04$ in./turn. This is in good agreement with the computer model results. We verified that the rate of growth, for both oscillations, varies linearly with the slope of the twist and with the displacement in the x-direction.

Using the same initial conditions for the particle and the same slope for the twist in the median plane, but $R_0 = \bar{R}_{144}$ MeV, we repeated our static case, away from the resonance, at 144 MeV. The behaviour of the particle, in that case, is shown in Fig. 4.4. The radial motion is almost unaffected. However, in the vertical motion, the maximum amplitude is reduced to 0.45 in. The beat period is also reduced to approximately

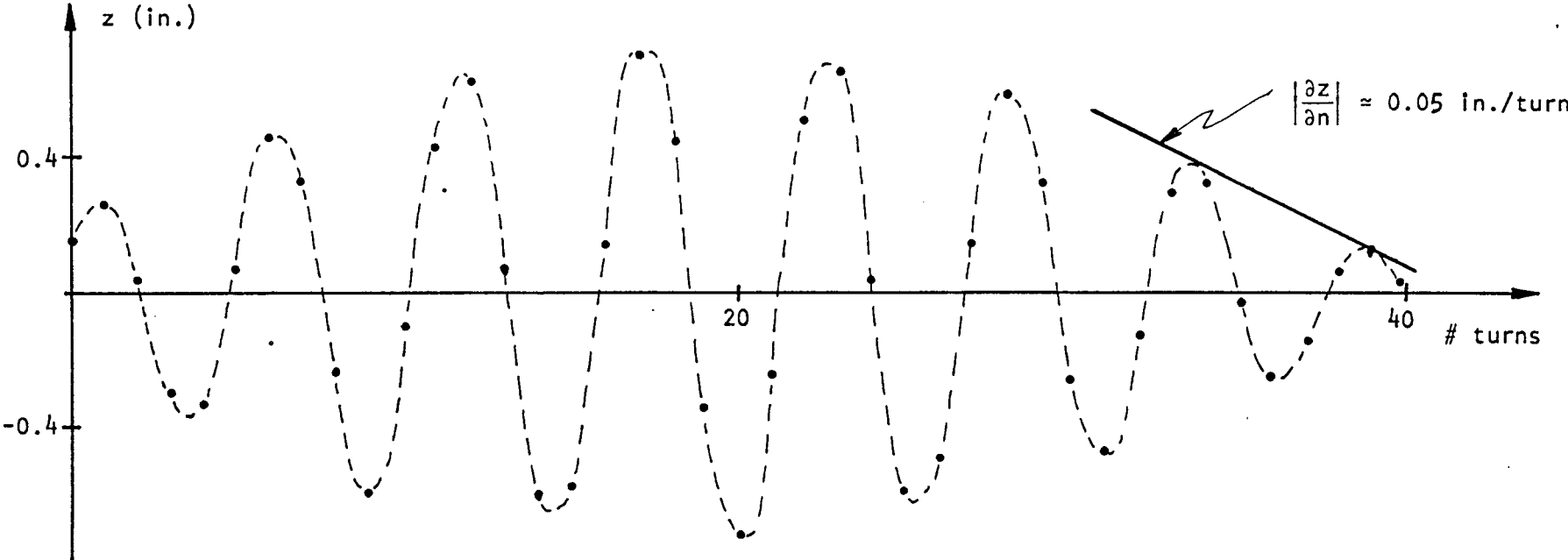
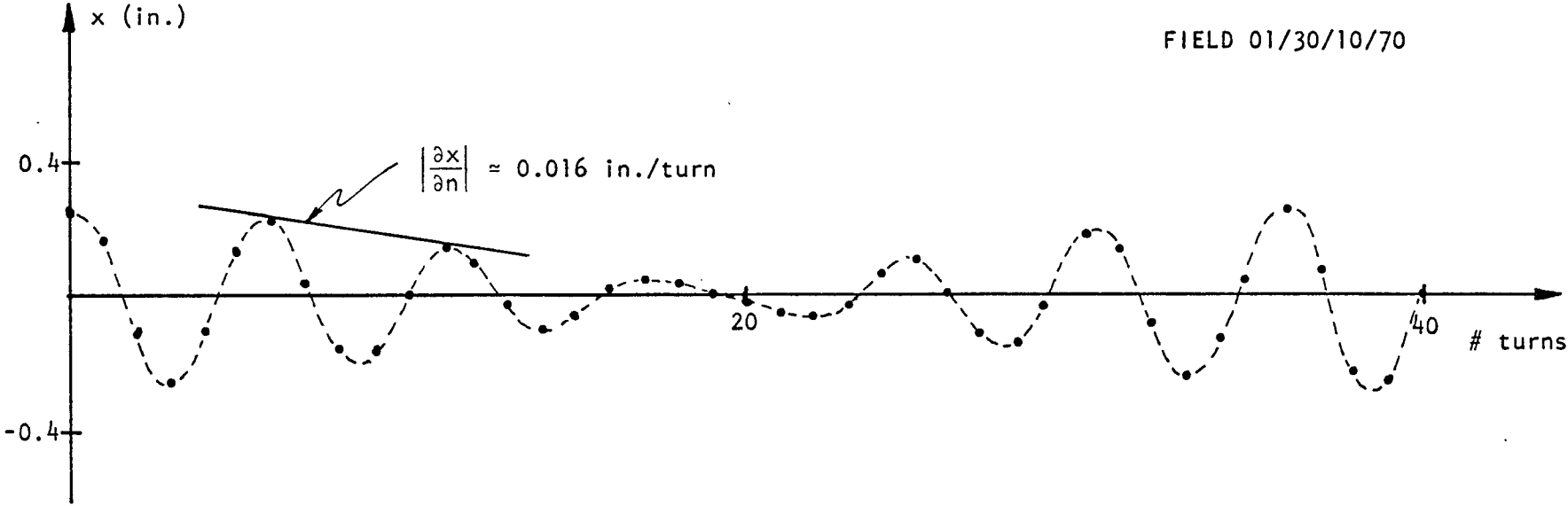


Fig. 4.3. Radial and vertical betatron oscillations at 153 MeV (on resonance) when a first harmonic twist with a slope of $\alpha = 0.02$ rad and $R_0 = R_{153}$ MeV is present

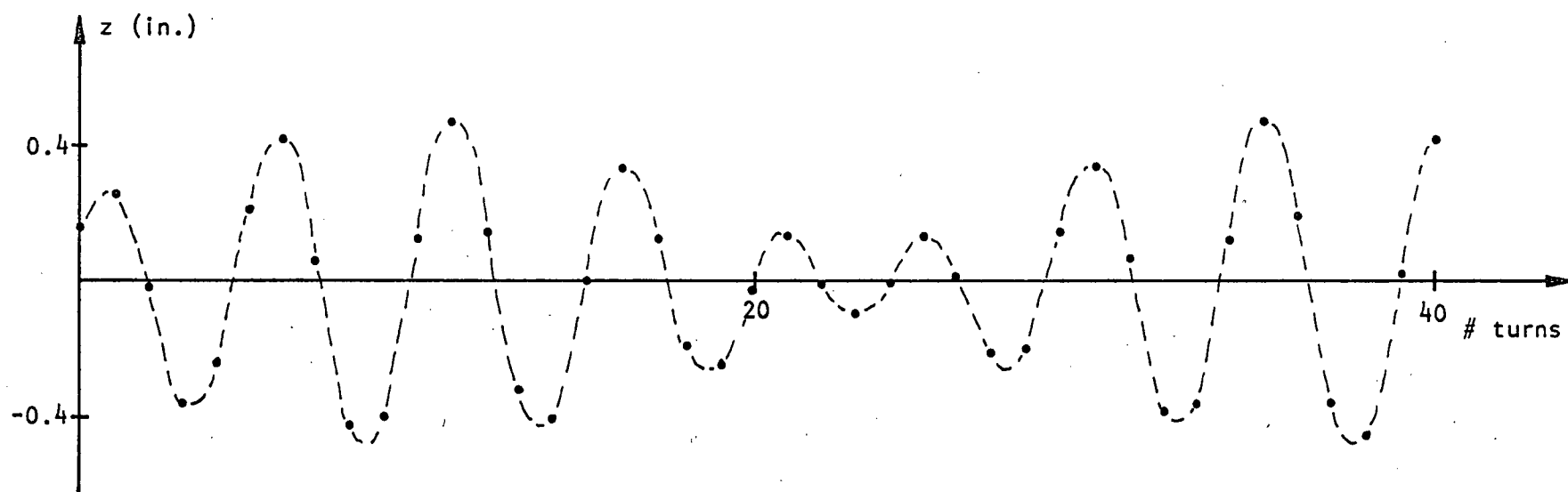
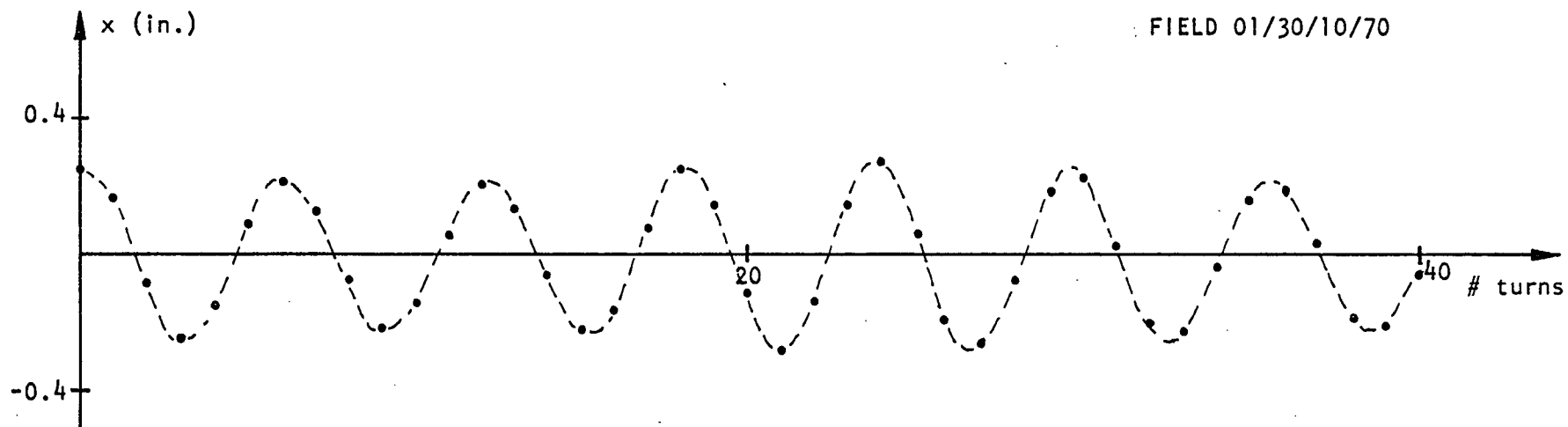


Fig. 4.4. Radial and vertical betatron oscillations at 144 MeV (10 MeV below resonance) when a first harmonic twist with a slope of $\alpha = 0.02$ rad and $R_0 = \bar{R}_{144}$ MeV is present

26 turns. A very crude estimate of the beat period, in that case, may be obtained from Eq. 4.11 and Eq. 4.12. In Eq. 4.12, the detuning term $\Delta\nu = \nu_x - \nu_z - 1$ is equal to zero when exactly on resonance. Away from the resonance, this term dominates if we have small twist angles, so that

$$\phi' \approx -\Delta\nu. \quad (4.24)$$

When ϕ changes by π , Eq. 4.11 tells us that the modulation amplitude goes from a maximum to a minimum. This turn-over occurs after n turns such that

$$2\pi n\phi' = \pi \quad (4.25)$$

or, using Eq. 4.24,

$$n = -1/(2\Delta\nu). \quad (4.26)$$

One complete beat cycle occurs for a change in ϕ of 2π . At 144 MeV, $\Delta\nu$ is approximately equal to -0.03 and, using Eq. 4.26, this corresponds to a beat period of approximately 33 turns.

Finally, we accelerated our particle backward from the resonance at 153 MeV to 125 MeV, with the conditions $\alpha = 0.02$ rad and $R_0 = \bar{R}_{153}$ MeV. The results are shown in Fig. 4.5. In this case, also, the change in the x-motion is relatively small. The maximum amplitude for the vertical oscillation is 0.6 in. compared to 0.7 in. when on resonance. The rate of growth is the same as in the static run. As we expect, the beat period decreases as we move away from the resonance. The particle goes through three complete beat periods in about 70 turns. In the case where the slope of the twisted median plane is reduced to $\alpha = 0.005$ rad, the frequency shift, and hence the beat cycle, is determined by $\Delta\nu$ as a function of energy, since $\Delta\nu$ dominates in Eq. 4.12 after only two or three turns. We observed, in that case, a turn-over of the oscillation after 17 turns. The effective width of the resonance, defined as twice the

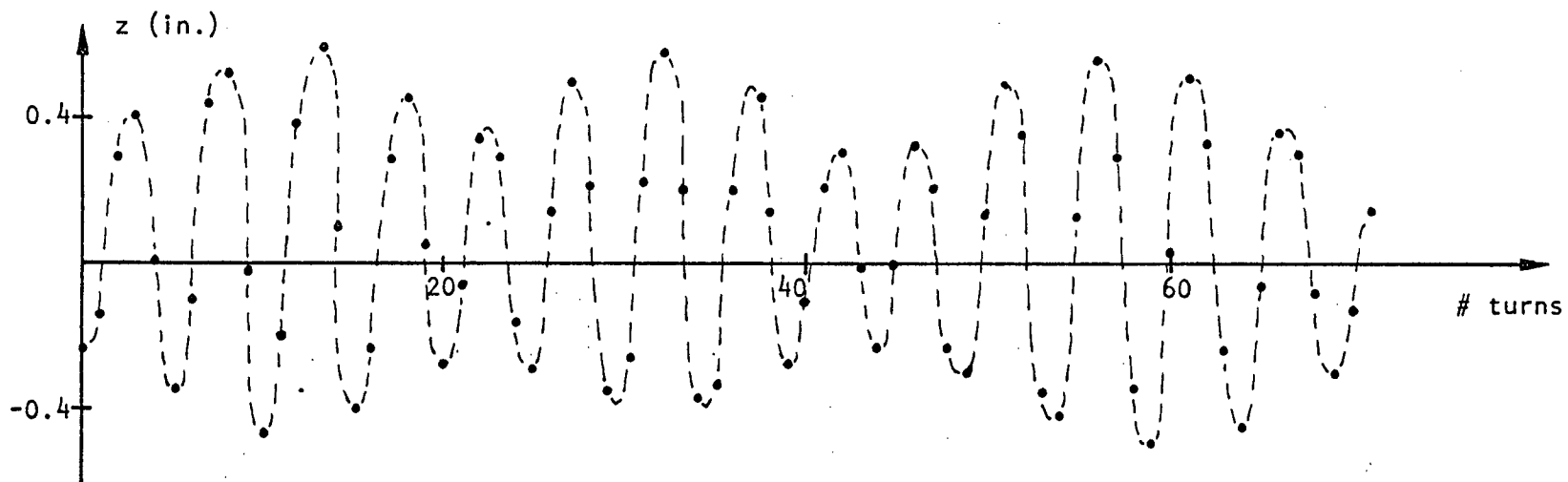
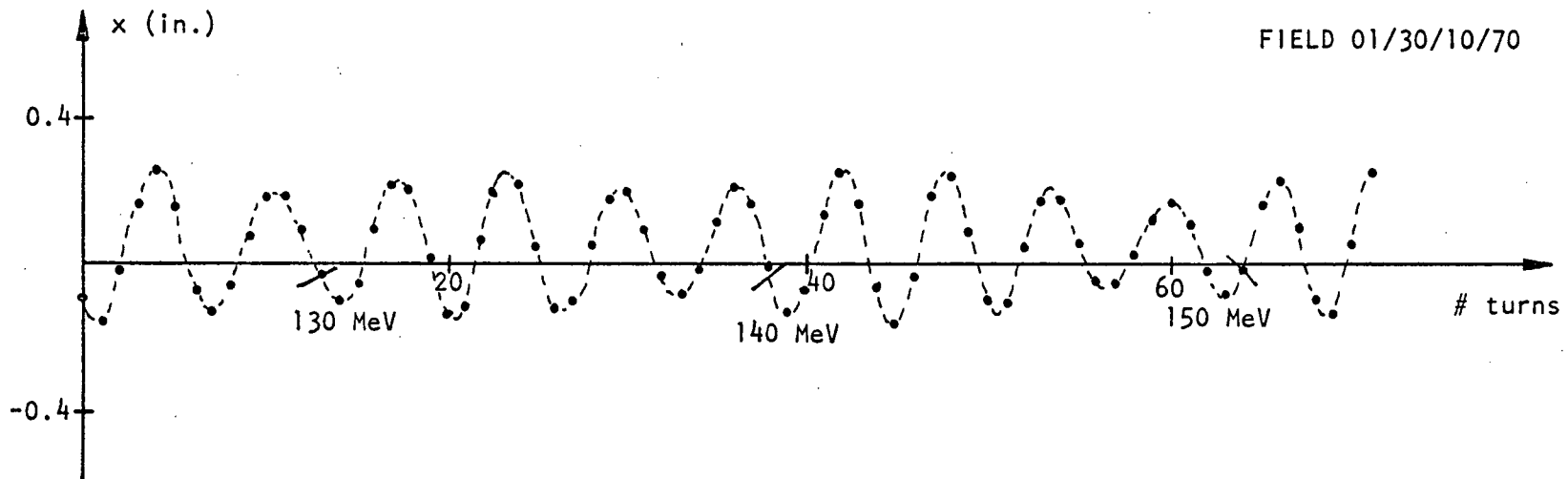


Fig. 4.5. Radial and vertical betatron oscillations at $125 \text{ MeV} \leq E \leq 153 \text{ MeV}$ when a first harmonic twist with a slope of $\alpha = 0.02 \text{ rad}$ and $R_0 = R_{153} \text{ MeV}$ is present (obtained from backward runs)

number of turns, on each side of the resonance, it would take the particle to reach the same maximum amplitude in the case of linear growth, is approximately equal to 24 turns. These 24 turns define an effective width of the resonance for use when α is small.

4.3 Tolerances

Various aspects of the resonance may be considered to set the tolerances associated with it. First of all, if the slope of the twisted median plane is large enough to produce a complete transfer of energy between the two motions, then some particles will leave the resonance region with all the energy in either the horizontal or the vertical motion. These maximum amplitudes depend, as we said, on the total available energy J_0 , which, in turn, depends on the initial amplitudes of the oscillations. Some of these worst cases are illustrated in the following table:

x_{initial}	z_{initial}	Total Energy J_0	x_{final}	z_{final}
x_0	~ 0	$0.6 x_0^2$	x_0	$2.45 x_0$
~ 0	z_0	$0.1 z_0^2$	$0.41 z_0$	z_0
x_0	x_0	$0.7 x_0^2$	$1.08 x_0$	$2.65 x_0$
x_0	$2x_0$	$1.0 x_0^2$	$1.29 x_0$	$3.16 x_0$
x_0	$10x_0$	$10.6 x_0^2$	$4.2 x_0$	$10.3 x_0$

Table 4.1. Maximum betatron amplitudes (either x_{final} or z_{final}) below and above the resonance $\nu_x - \nu_z = 1$ when $\nu_x \approx 1.2$ and $\nu_z \approx 0.2$.

For example, in the case of separated turn acceleration at high energy, where the turn separation is approximately 0.06 in., the maximum amplitude

of the radial oscillation we can tolerate is $x \leq 0.03$ in. Then, if we assume that before entering the resonance the oscillation amplitude is 0.01 in. and that the transfer of energy into the radial motion builds up an oscillation of 0.03 in., Eq. 4.5 tells us that the amplitude of the vertical oscillation, just before the resonance, must be kept below 0.07 in. If the initial x_0 is 0.02 in., then the initial vertical amplitude must be smaller than 0.055 in. Similarly, if for high current poor resolution experiments we are willing to accept a vertical amplitude of 0.5 in. after the resonance, then we can tolerate some particles with a radial oscillation of 0.19 in. amplitude before the resonance, provided the vertical amplitude before the resonance is also not larger than 0.19 in. If these restrictions are acceptable, then we need not worry about the magnitude of the first harmonic twist in the median plane.

The tolerance may, on the other hand, be set according to the maximum acceptable increase in the amplitudes of the oscillations. We found that the rate of growth of the oscillations varies linearly with the tilt angle and that the width of the resonance, for small values of α , is in this case approximately equal to 24 turns. Then, if we assume that the maximum tolerance increase in z is equal to 0.10 in., or 0.004 in./turn, we find that the corresponding maximum twist angle of the two sectors is $\alpha = 0.003$ rad, or 0.2 deg where $x_0 = 0.2$ in. Similarly, if we restrict the increase in the radial oscillation to 0.01 in., the tolerance on the slope of the twist in the median plane is equal to $\alpha = 0.002$ rad, or 0.1 deg, for $z_0 = 0.2$ in.

5. THE RESONANCE $\nu_x = 1.5$

5.1 The Intrinsic Resonance $\nu_x = 6/4$

The resonance $\nu_x = 6/4$ will be encountered at an energy of approximately 435 MeV and a radius of 298 in. In the absence of error fields, this intrinsic resonance of fourth order (in the Hamiltonian) may be traversed successfully since the particle spends only a few turns in the resonance region so that little growth takes place. To determine the stability limit for the oscillation, we look at the radial phase space, as illustrated in Fig. 5.1 where we show the case of an ion at 425 MeV with $\nu_x = 1.487$, using the field 01/18/02/70. Each dot represents the position of the particle after every second turn in the machine. The arrows show the direction of flow in phase space for particles displaced from the equilibrium orbit. Inside the region defined by the four unstable fixed-points, the orbits are closed and the oscillations are stable. Outside that region, the radial motion becomes unstable and the amplitude of the oscillation increases. The quadrilateral joining the unstable fixed-points essentially determines the size of the stability region. The region of linear motion, where the particle precesses around an ellipse, extends over approximately half the size of the stable region.

At other energies, the positions of the unstable fixed-points will be changed. Fig. 5.2 shows the motion of these fixed-points as a function of energy for the field 01/18/02/70. The lines have been drawn to show the changing size of the stability region as the energy changes. The stable region has its minimum at approximately 434 MeV; that is where $\nu_x = 1.5$. In this case, the limit of stable radial oscillation is less than 0.2 in. but the particle spends only three or four turns in that region. For other fields, the size of the stability region may be larger or smaller. As

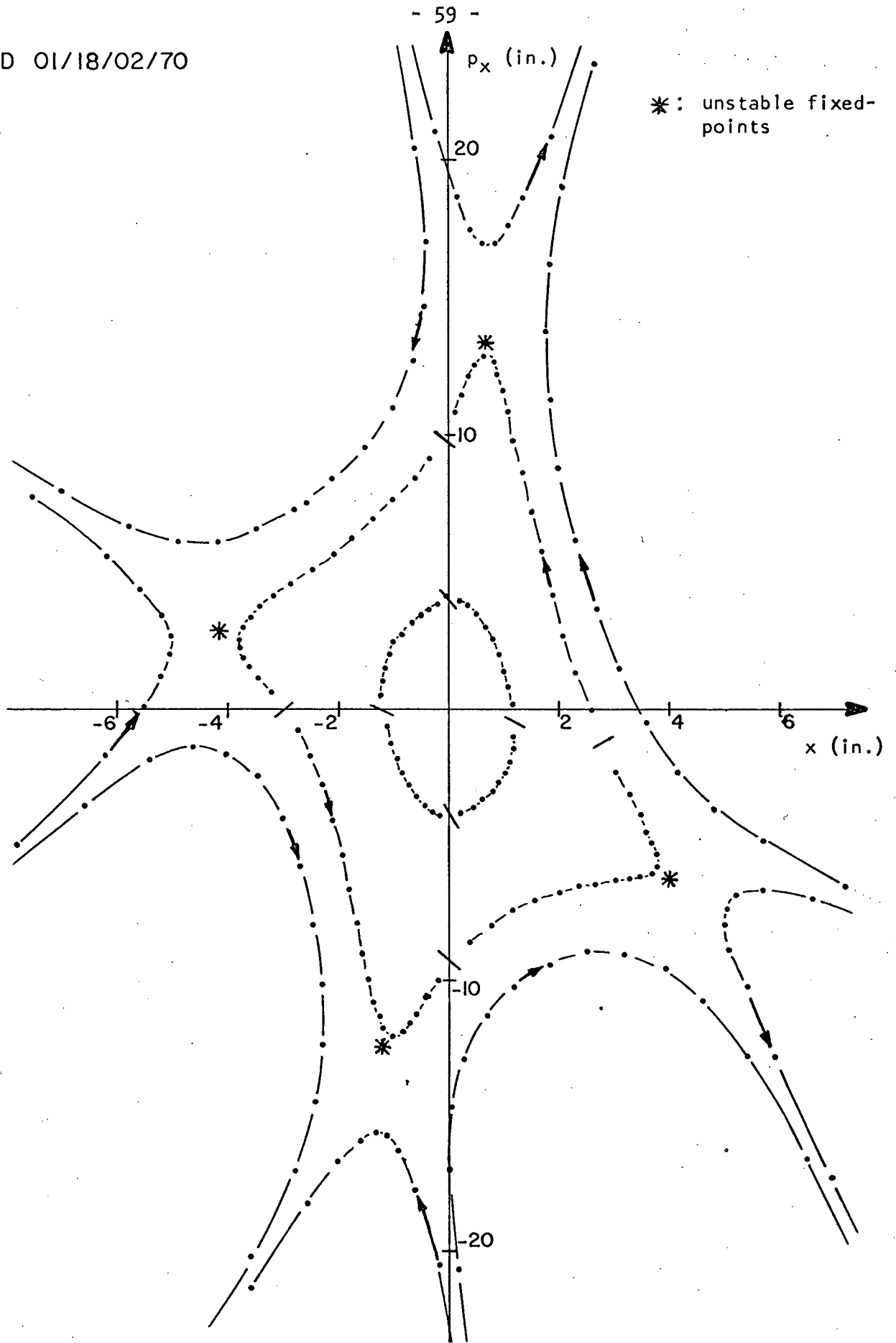


Fig. 5.1. Phase space plot at 425 MeV and $\nu_x = 1.487$ for ions of 0 deg RF phase (resonance $\nu_x = 6/4$)

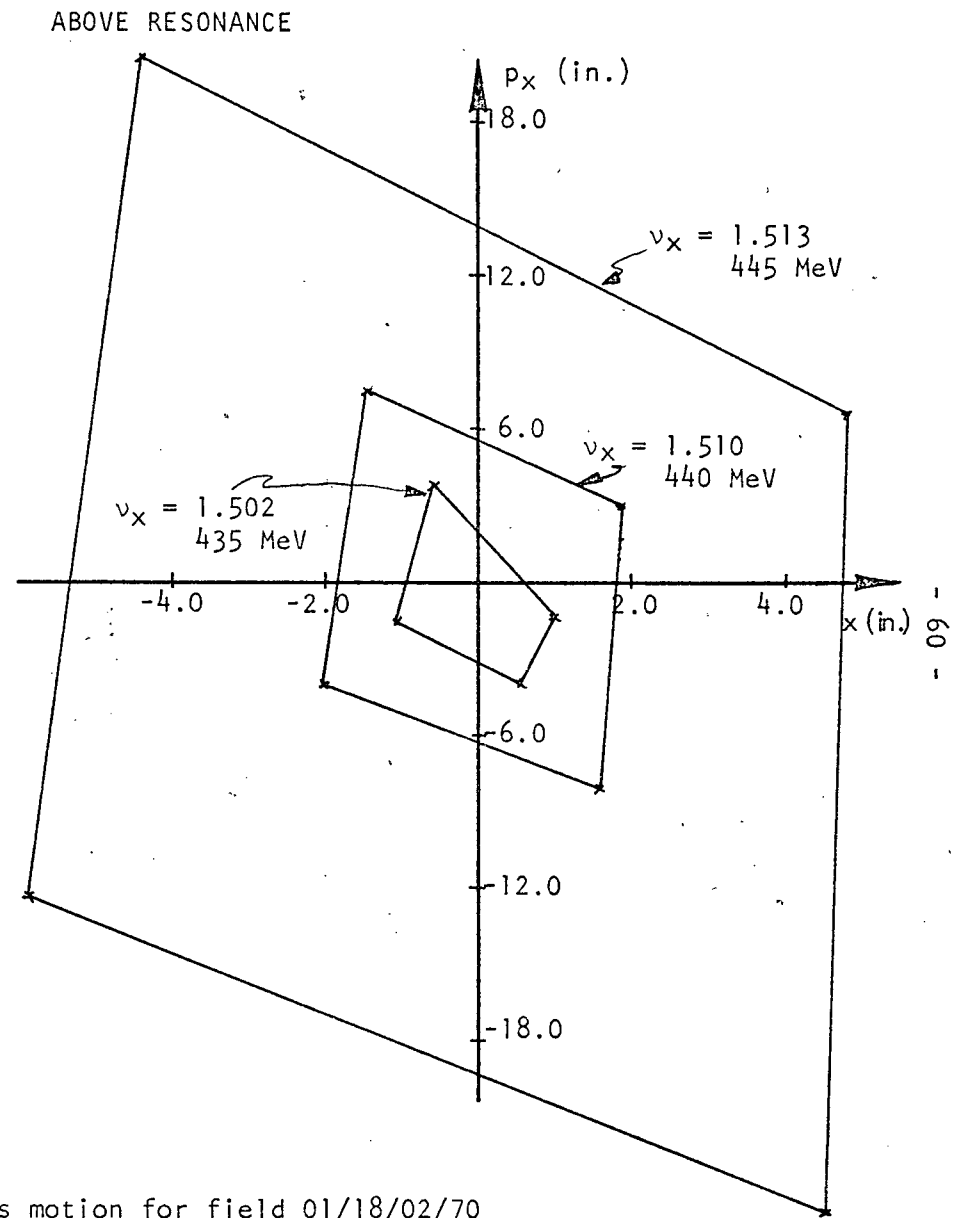
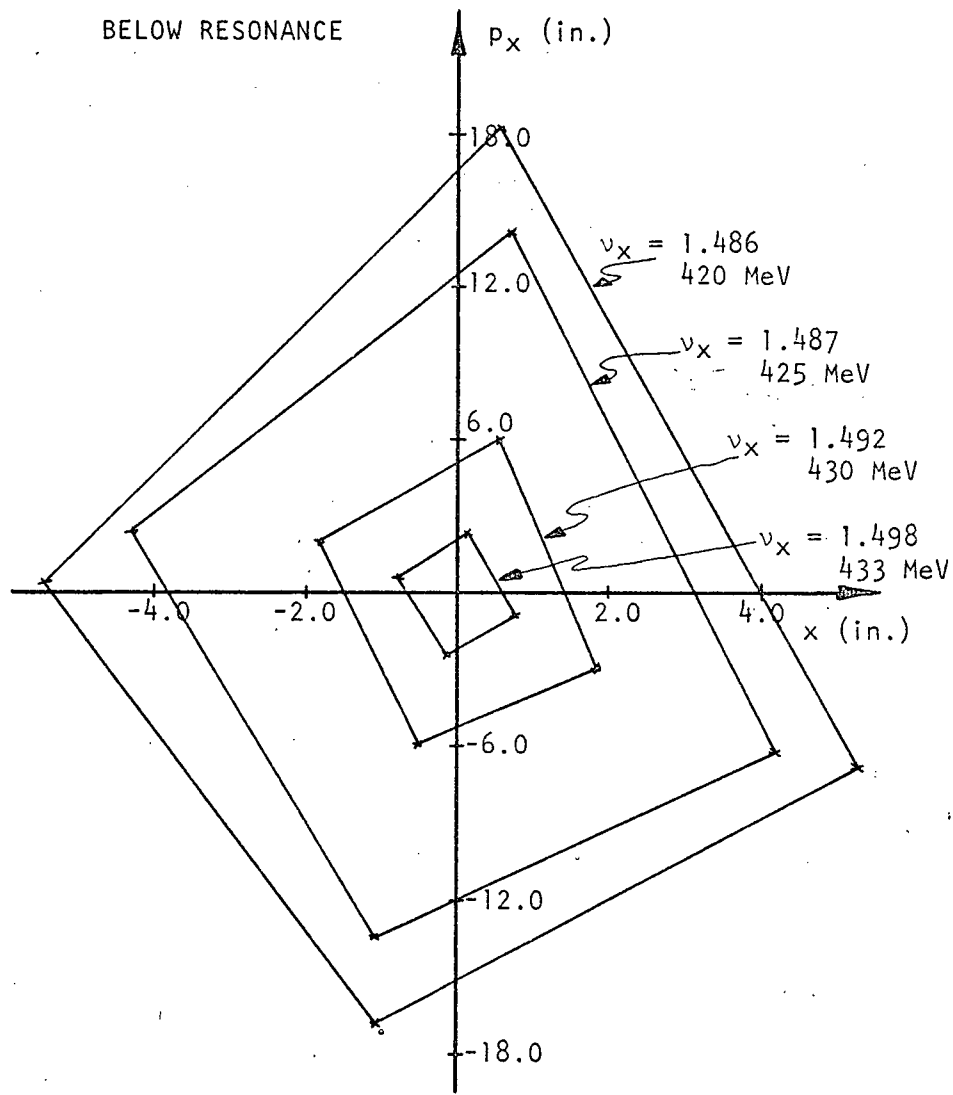


Fig. 5.2. Unstable fixed-points motion for field 01/18/02/70

seen in Fig. 5.3, the limit of stable oscillation for the field 02/09/07/71 is about 2.0 in. compared to 0.2 in. for our previous field when $\nu_x = 1.498$. The difference is thought to be due to higher derivatives of the magnetic field that drive the resonance. Fig. 5.3 implies, as accelerated GOBLIN runs will show in Section 5.2.3, that when no field errors are present, the beam may easily cross the resonance region.

5.2 The Resonance $\nu_x = 3/2$

5.2.1 Introduction

The resonance $\nu_x = 3/2$ is, in first order, driven by a third harmonic imperfection with a radial gradient. Such an imperfection gives rise, in the equations of motion, to a term similar to the third term on the right-hand side of Eq. 2.21. A third harmonic whose amplitude is constant with radius would also drive the resonance $\nu_x = 3/2$. However, the amplitude required to render the radial motion unstable is of the order of 10 G and should not occur in practice.

When the third harmonic gradient is introduced, the frequency of the radial oscillation is shifted. This shift in ν_x is conveniently measured by simply considering the trace (T_R) of the R-transfer matrix. We note that ν_x is derived from T_R by using

$$\nu_x = \frac{N}{2\pi} \cos^{-1}(T_R/2) \quad (5.1)$$

where N is the number of sectors in the machine. If the amplitude of the gradient is large enough to shift ν_x to an imaginary value, the amplitude of the radial oscillation will, after a few turns, grow exponentially with time, with an exponent proportional to $\cosh^{-1}(T_R/2)$. We can then measure the approximate rate of growth by simply looking at the values of T_R at different energies.

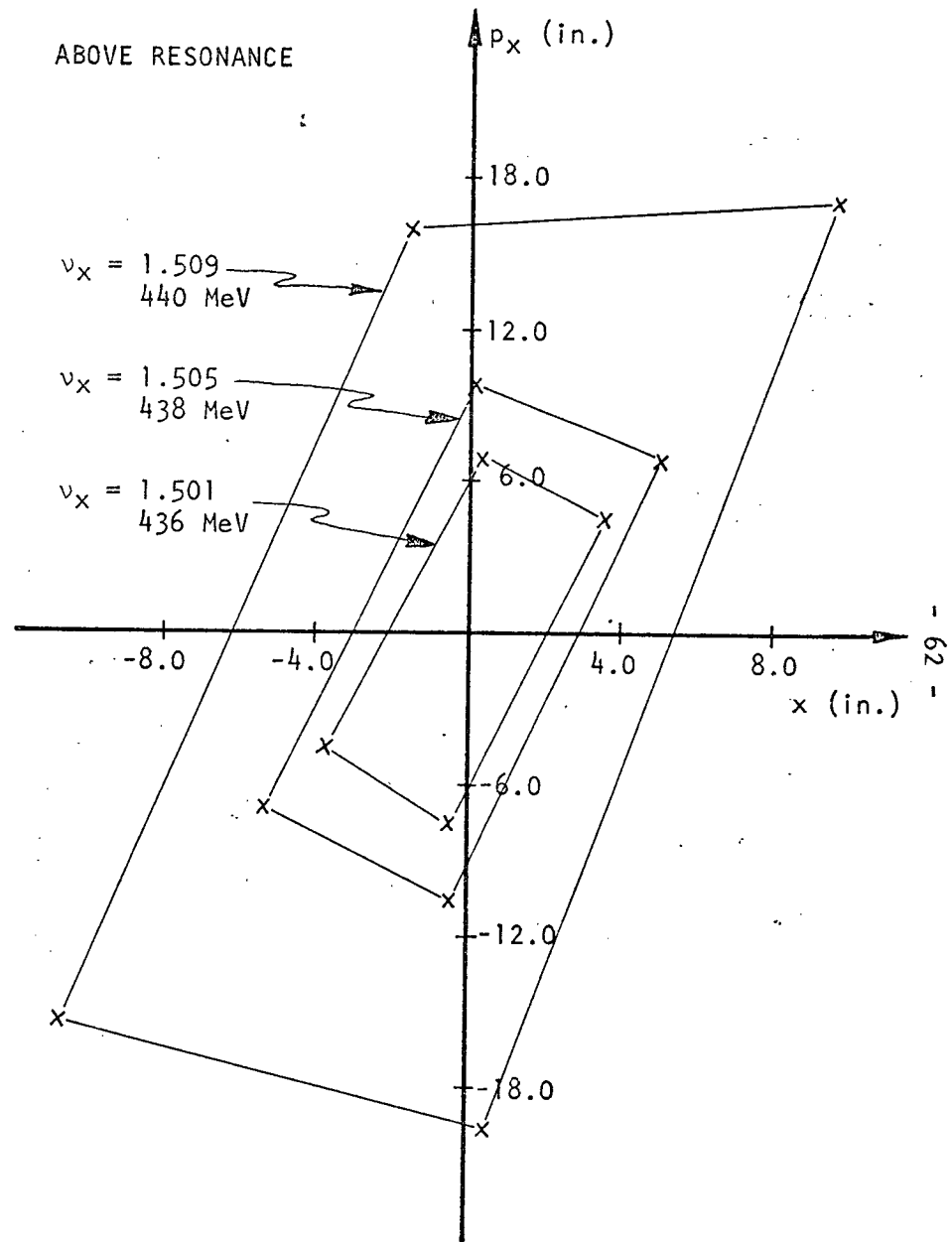
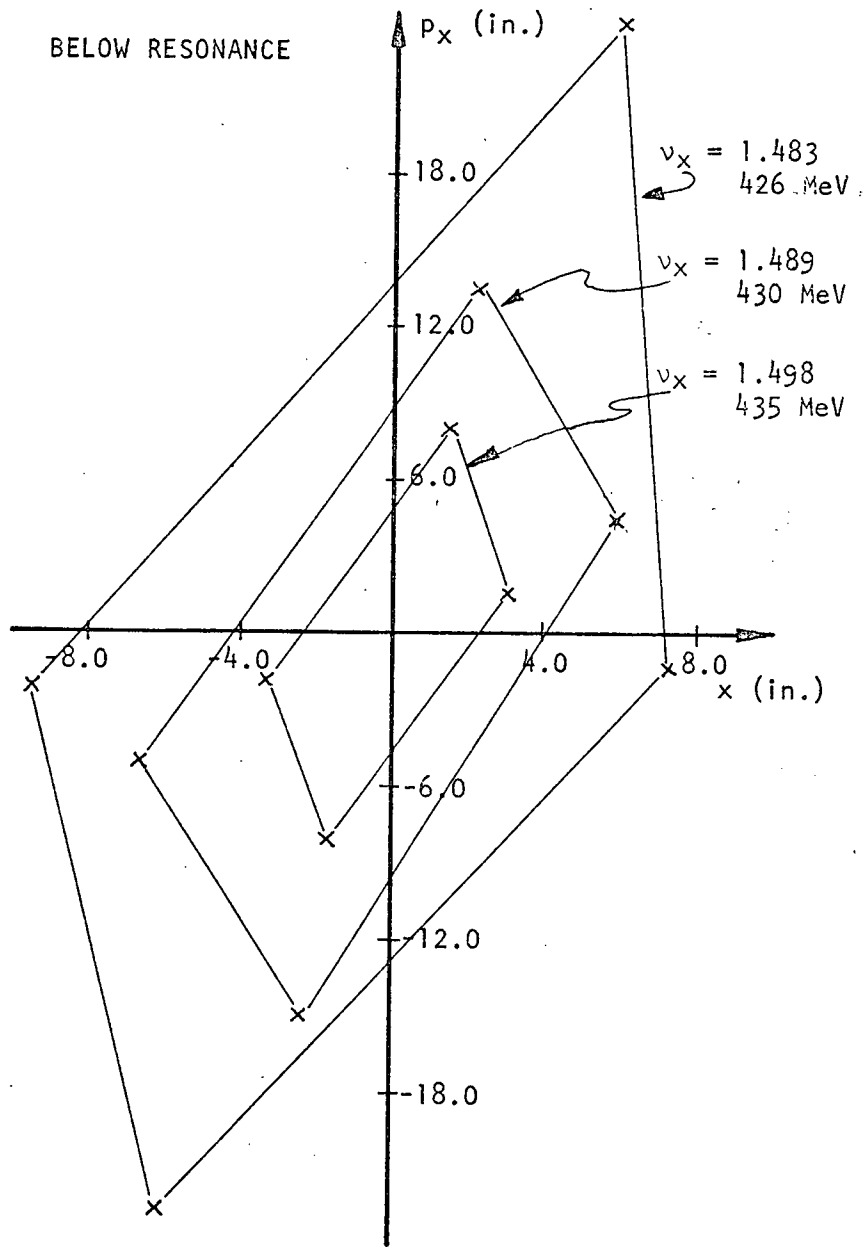


Fig. 5.3. Unstable fixed-points motion for field 02/09/07/71

5.2.2 Calculations

All calculations were done using the field 02/09/07/71. The third harmonic gradient, with three free parameters, may be written

$$\begin{aligned} B_3(R, \theta) &= 0 & R \leq R_S \\ B_3(R, \theta) &= A_3 (R - R_S) \cos(3\theta - \phi_3) & R > R_S \end{aligned} \quad (5.2)$$

where A_3 is the amplitude of the gradient, R_S is the starting radius and ϕ_3 is the bump phase. The phase angle of the bump may be constant with radius or may have the same spiral as the phase of the sixth harmonic. It was found that the frequency shift was quite sensitive to the phase parameter. This is seen on Fig. 5.4 where we have shown, as a function of the bump phase angle, the value of the trace at 433 MeV and 435 MeV, which is the energy at which T_R almost reaches its maximum value. The amplitude of the third harmonic gradient was 0.4 G/in. in this case. The greatest frequency shift, and hence the strongest radial instability, occurs when the bump phase leads the phase of the sixth harmonic by approximately 12 deg. When the phase of the third harmonic is constant with radius, the maximum shift in ν_x occurs when $\phi_3 \approx 15$ deg. In both cases, the magnitude of the frequency shift is of the same order. These results are different from those obtained by Hopp and Richardson¹² in a similar analysis. They found that the frequency shift was more important when the bump was exactly in phase with the sixth harmonic.

The starting radius is also a sensitive parameter. As shown in Fig. 5.5, displacement of 10 in. in R_S changes the width of the resonance, i.e. the range of energy values for which ν_x is imaginary, by approximately 25%. In the following, the starting radius was fixed at 287.5 in., about 10 in. below the 435 MeV radius. Using the pessimistic case of $\phi_3 = \phi_6 + 15$ deg for the bump phase, we considered various gradient amplitudes and

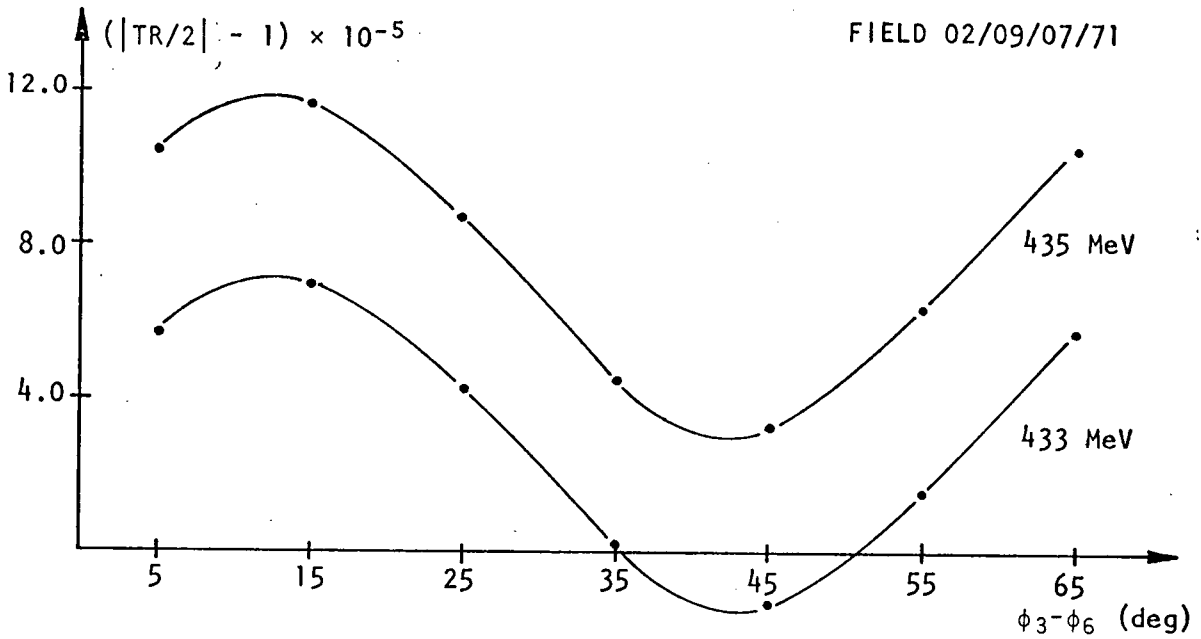


Fig. 5.4. The effect of the bump phase parameter on the width of the resonance in the case of a 0.4 G/in. third harmonic gradient with $R_s = 287.5$ in.

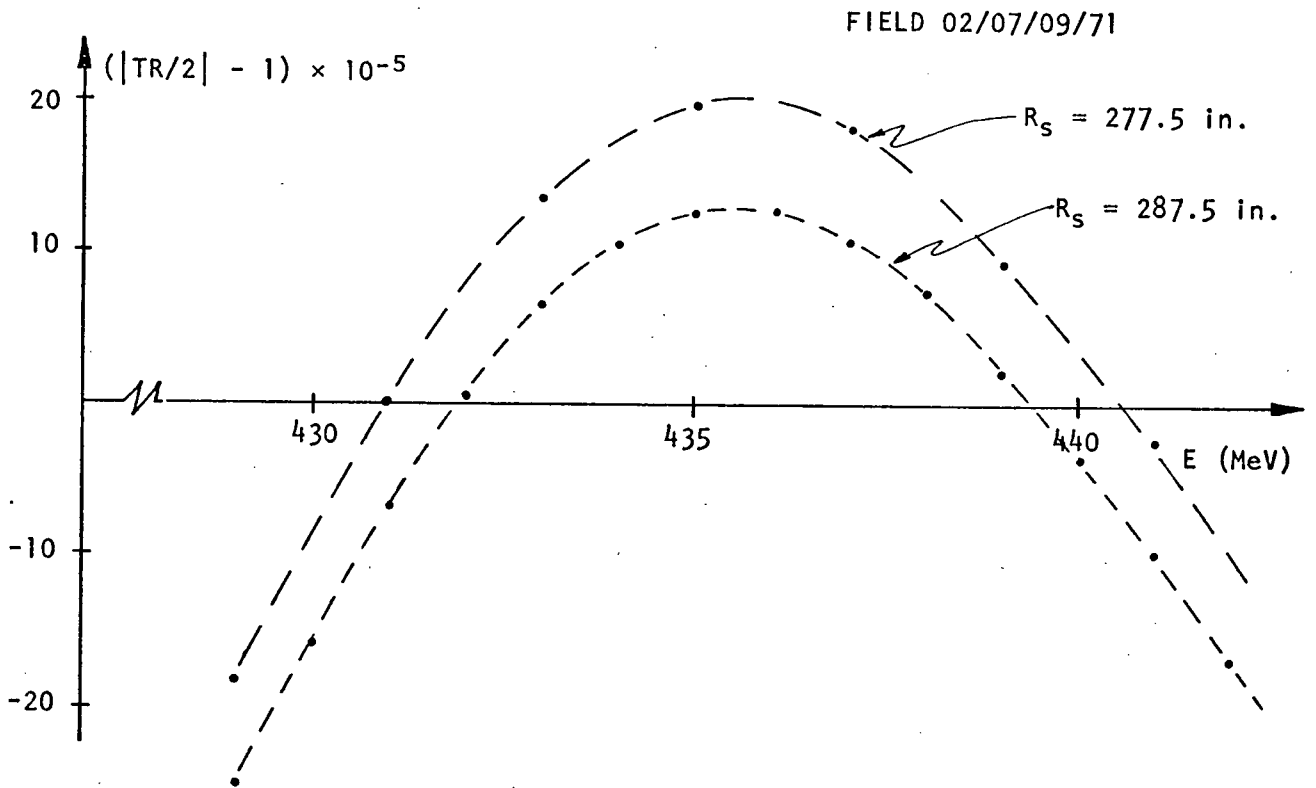


Fig. 5.5. The effect of the starting radius parameter on the width of the resonance in the case of a 0.4 G/in. third harmonic gradient with $\phi_3 = \phi_6 + 15$ deg

FIELD 02/09/07/71

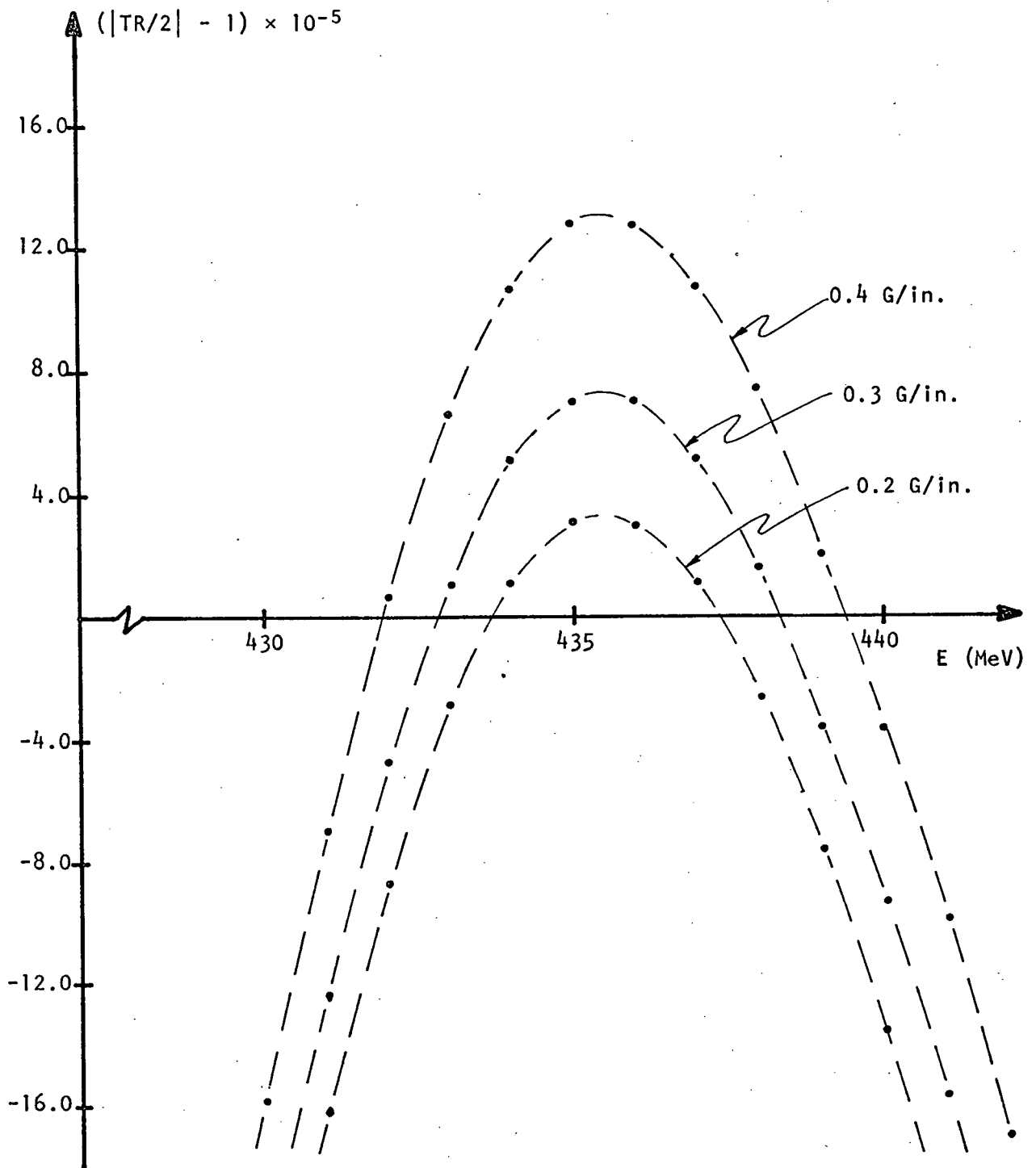


Fig. 5.6. The effect of various gradient amplitudes on the width of the resonance when $R_s = 287.5$ in. and $\phi_3 = \phi_6 + 15$ deg

measured, in each case, their effect on the width of the resonance. The results are shown on Fig. 5.6. A gradient of 0.4 G/in. amplitude gives rise to an unstable region with a width of approximately 9 MeV and a peak value for the imaginary ν_x of 0.008i at 435 MeV. Similarly, the unstable region due to a 0.2 G/in. gradient extends over 5 MeV. We then looked at the effects of such gradients on the rate of growth of the radial oscillation and on the radial phase space configuration.

5.2.3 Static and Accelerated Phase Space with Third Harmonic Gradient

Upon introduction of a third harmonic gradient, two of the unstable fixed-points in a static phase space diagram move inwards while the other two go outwards. The general configuration of the phase space is then altered and the size of the stability region is reduced. The effect of a 0.5 G/in. gradient on an ion at 430 MeV, using the field 01/18/02/70, is shown in Fig. 5.7. If we compare the positions of the unstable fixed-points in this case with their previous positions, as seen in Fig. 5.2, when no third harmonic was present, we observe that the two unstable fixed-points along the p_x -axis have moved inwards. The stability region is also slightly stretched in the x -axis direction. With a larger gradient, two of the unstable fixed-points will eventually coincide and no stable region will be left. As illustrated in Gordon and Hudec,¹³ the detailed shape of the flow lines depends on the phase of the gradient.

We finally considered the influence of a third harmonic gradient on the amplitude of the radial oscillation, and hence on the beam quality. We accelerated eight particles with 0 deg RF phase from 425 MeV to 445 MeV, through the resonance region. This was done with gradients of 0.2 G/in. and 0.4 G/in. amplitude and phase of $\phi_3 = \phi_6 + 15$ deg superimposed on the

FIELD 01/18/02/70

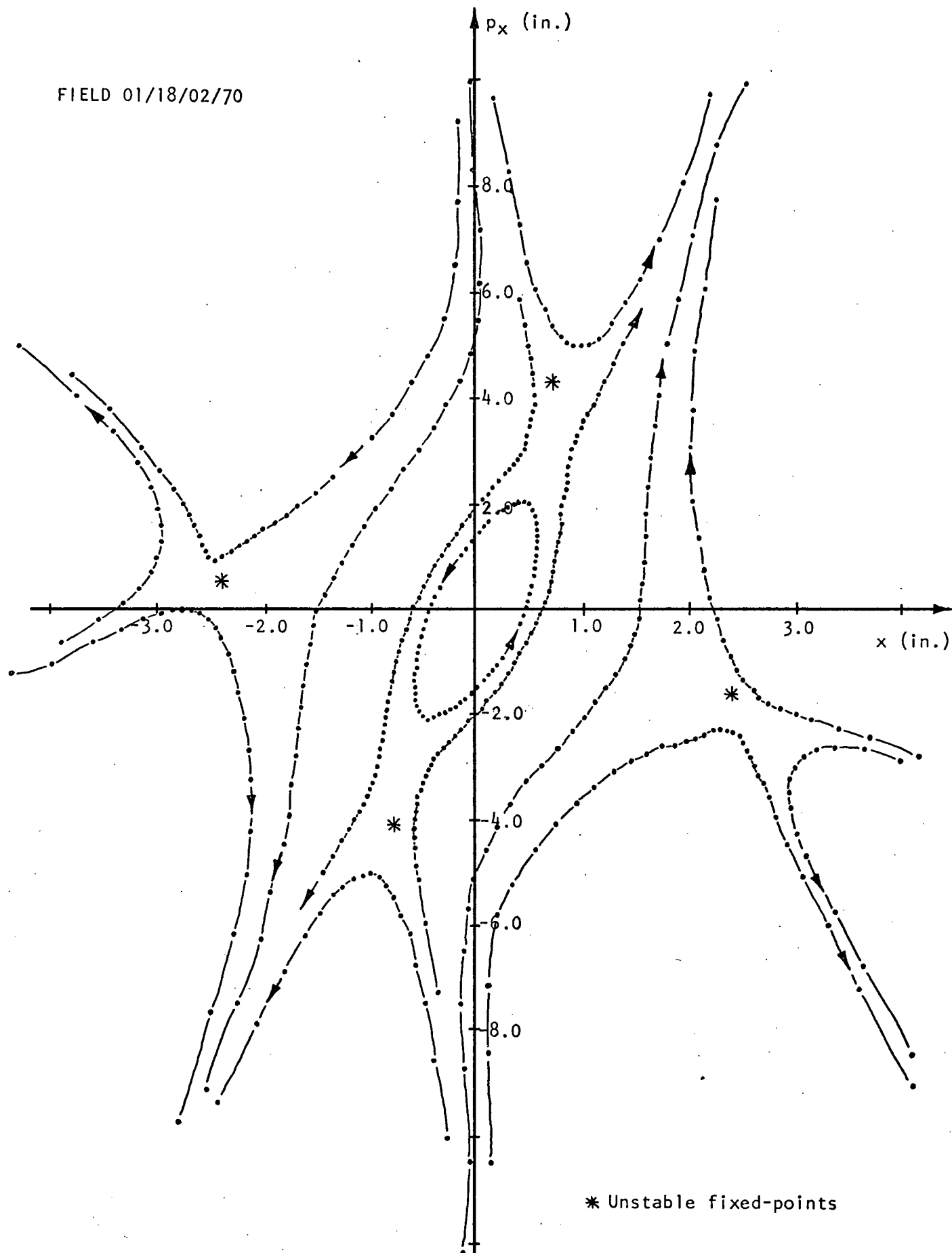


Fig. 5.7. Phase space plot at 430 MeV and $v_x = 1.492$ for ions of 0 deg RF phase when a 0.5 G/in. third harmonic gradient is present

smooth magnetic field 02/09/07/71. In each case, the initial positions of the particles in phase space defined an ellipse whose area corresponded to a beam emittance of approximately 0.05π in. mrad at 425 MeV. Below the resonance, we assume that the emittance precesses around a static ellipse that it fills. In the resonance region, the emittance stretches along the two opposite directions of the flow lines in phase space. Then, above the resonance, the stretched emittance is recaptured into stable motion and precesses around a larger ellipse that it does not fill. Thus, the effective phase space area occupied by the beam is increased.

When no third harmonic gradient is present, the effective emittance, below and above the resonance, remains approximately constant. The static ellipse at 441 MeV is shown in Fig. 5.8, together with the corresponding accelerated ellipse at the same energy. When a 0.2 G/in. gradient is added to the magnetic field, the effective area occupied by the beam at 441 MeV is increased by a factor three. This is shown in Fig. 5.9. Also shown are the stretched emittances at 440 MeV and 444 MeV, obtained in the accelerated GOBLIN runs. For ions with RF phases other than 0 deg, the ellipses in phase space are more stretched since the ions make more turns in the resonance region. They also make more turns to reach a given energy above the resonance and so precess through different angles. This precessional mixing effect makes the effective emittance shown on Figs. 5.8 to 5.10 the real beam emittance presented to an extraction mechanism. On Fig. 5.9, the stretching of the beam emittance for a single phase is of the order of 20%, and the maximum amplitude of the radial oscillation is approximately 0.15 in. This was considered the worst that could be accepted. When a 0.4 G/in. gradient is present, the area of the static ellipse at 441 MeV is increased by one order of magnitude, as illustrated

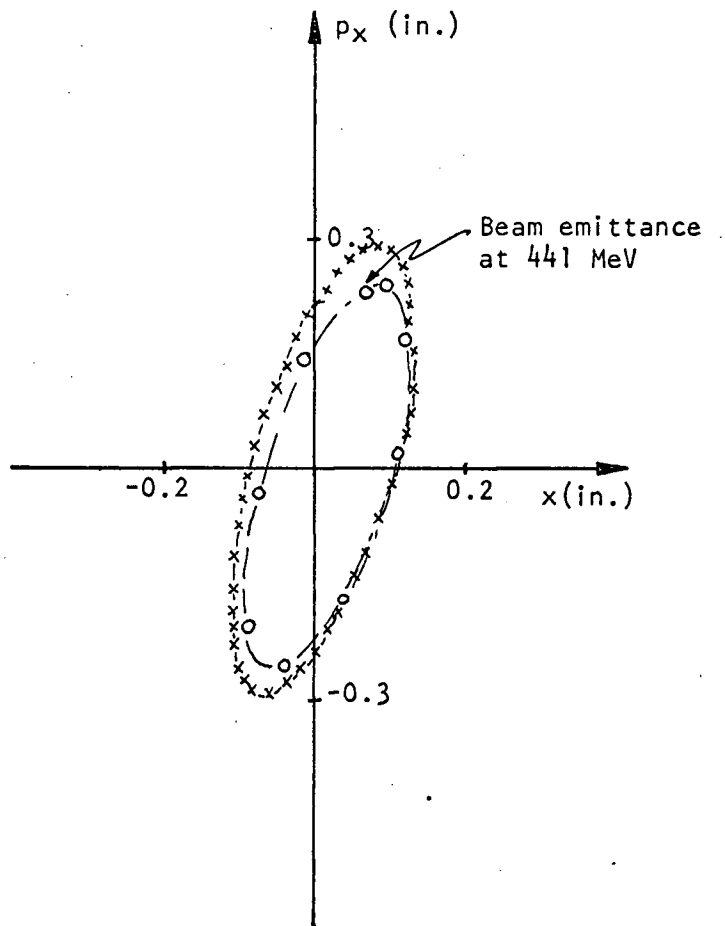


Fig. 5.8. Effective phase space area occupied by the beam at 441 MeV when no third harmonic gradient is present. The beam emittance is obtained from the accelerated runs.

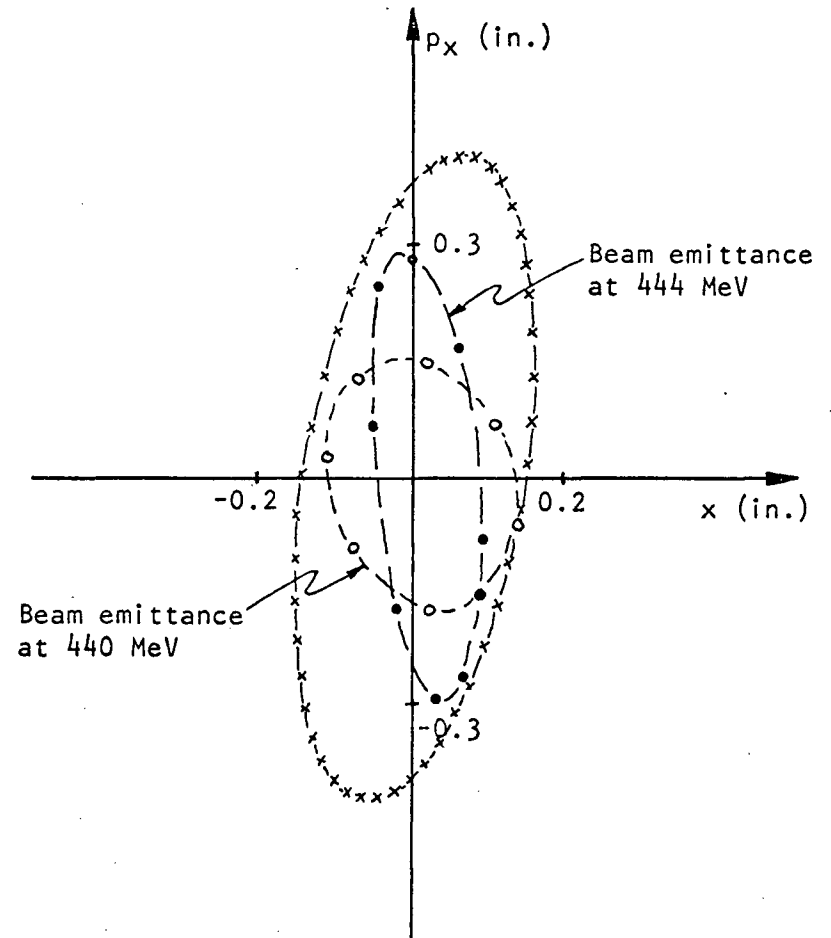


Fig. 5.9. Effective phase space area occupied by the beam at 441 MeV when a third harmonic gradient of 0.2 G/in. amplitude is present. The beam emittances are obtained from the accelerated runs.

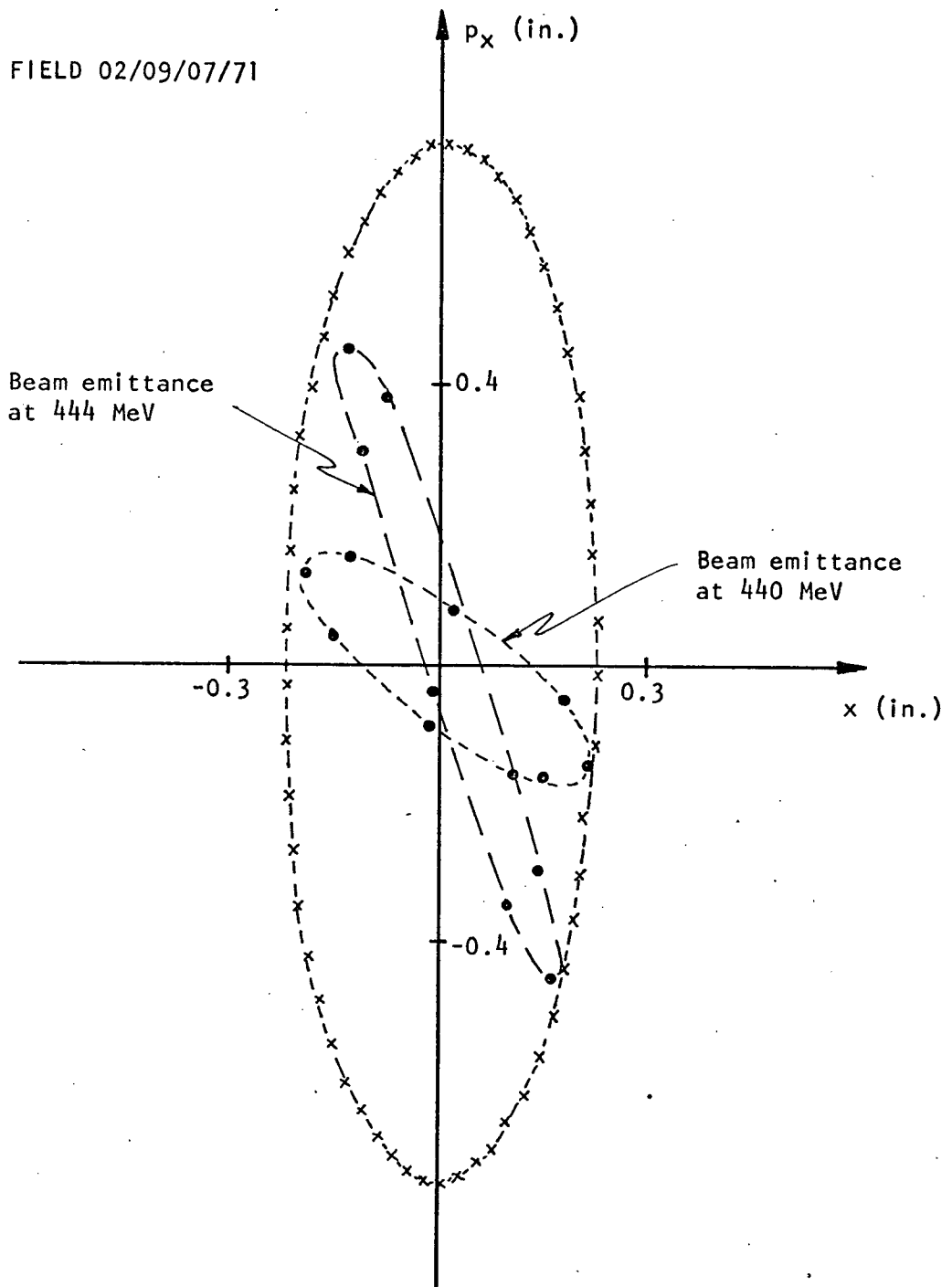


Fig. 5.10. Effective phase space area occupied by the beam at 441 MeV when a third harmonic gradient of 0.4 G/in. amplitude is present. The beam emittances are obtained from the accelerated runs.

in Fig. 5.10. The emittance is also stretched by a factor two. These conditions, though stable, would lead to a very poor beam quality.

REFERENCES

1. J.B. Warren, IEEE Trans. Nucl. Sci. NS-18, 272 (1971)
2. H. Thomas, Phys. Rev. 54, 580 (1938)
3. D.W. Kerst, J.L. Laslett *et al.*, CERN Symposium on High Energy Accelerators and Pion Physics, 1956, Proceedings Vol. I, p.32
4. W. Walkinshaw and N.M. King, "Linear Dynamics in Spiral Ridge Cyclotron Design", Harwell Report AERE-GP/R-2050 (1956)
5. P.A. Sturrock, Ann. Phys. (N.Y.) 3, 113 (1958)
6. R. Hagedorn, "Stability and Amplitude Ranges of Two-dimensional Non-linear Oscillations with Periodical Hamiltonian", CERN Report 57-1 (1957)
7. J.D. Lawson, Nucl. Instr. & Meth. 49, 114 (1967)
8. J.L. Bolduc and G.H. Mackenzie, IEEE Trans. Nucl. Sci. NS-18, 287 (1971)
9. M.K. Craddock, private communication (1971)
10. H.L. Hagedoorn and N.F. Verster, Nucl. Instr. & Meth. 18,19, 201 (1962)
11. W. Joho, "Extraction of a 590 MeV Proton Beam from the SIN Ring Cyclotron", SIN Report TM-11-8 (1970)
12. D.I. Hopp and J.R. Richardson, Nucl. Instr. & Meth. 44, 227 (1966)
13. M.M. Gordon and W.S. Hudec, "Effects of Field Imperfections on Radial Stability", MSUCP-11 (1961) unpublished
14. M.M. Gordon, private communication (1971)

APPENDIX A. MAGNETIC FIELD COMPONENTS IN THE PLANE OF MEASUREMENT

We start with Maxwell's equations and neglect the space charge forces so that

$$\text{rot} \vec{B} = 0 \quad (A.1)$$

$$\text{div} \vec{B} = 0 \quad (A.2)$$

We can then write \vec{B} as

$$\vec{B} = \text{grad}(\psi) \quad (A.3)$$

where ψ is the magnetic scalar potential and satisfies

$$\left(\frac{\partial^2}{\partial z^2} + \Gamma^2 \right) \psi = 0. \quad (A.4)$$

Γ^2 is the Laplacian in polar co-ordinates. Following a suggestion by M.M. Gordon,¹⁴ we express ψ as

$$\psi = C - \frac{z^2}{2!} \Gamma^2 C + \dots + zB - \frac{z^3}{3!} \Gamma^2 B + \dots \quad (A.5)$$

where $C(r, \theta)$ represents the imperfections destroying the median plane symmetry. The magnetic field components are written as

$$B_r = \frac{\partial C}{\partial r} + z \frac{\partial B}{\partial r} \quad (A.6)$$

$$rB_\theta = \frac{\partial C}{\partial \theta} + z \frac{\partial B}{\partial \theta}$$

$$B_z = B - z\Gamma^2 C - \frac{z^2}{2!} \Gamma^2 B.$$

If we have a flat median plane, C is everywhere zero and the above expressions are similar to our Eq. 2.13. In practice, $C(r, \theta)$ can be obtained from measuring $\partial B_z / \partial z$.

We now want to show that Eq. A.6 can be written in a form similar

to Eq. 2.17. We consider a symmetric magnet and rotate one sector by an angle α with respect to the plane of measurement, as shown in Fig. A.1. At point P with co-ordinates (r, z) and (R^*, Z^*) , we have

$$x = r - r_0 \quad (A.7)$$

$$R^* = r_0 + x \cos\alpha + z \sin\alpha \quad (A.8)$$

$$Z^* = z \cos\alpha - x \sin\alpha \quad (A.9)$$

so that

$$R^* \approx r + z\alpha \quad (A.10)$$

$$Z^* \approx z - x\alpha \quad (A.11)$$

We first consider the azimuthal component of the magnetic field in the rotated system. At a point A, on the median plane of the rotated system, where $Z^* = z - \alpha x = 0$, we have $B_\theta^* = 0 = B_\theta$. Then, from Eq. A.6 we obtain

$$\frac{\partial C}{\partial \theta} = -z \frac{\partial B}{\partial \theta} = -\alpha x \frac{\partial B}{\partial \theta}. \quad (A.12)$$

For the radial component of the magnetic field, we have

$$B_{R^*} = B_r \cos\alpha + B_z \sin\alpha \quad (A.13)$$

and, for $Z^* = z - \alpha x = 0$, we require $B_{R^*} = 0$ so that, with the use of Eq. A.6, Eq. A.13 becomes

$$B_r + \alpha B_z = \frac{\partial C}{\partial r} + \alpha x \frac{\partial B}{\partial r} + \alpha B - \alpha^2 x r^2 C - \dots = 0. \quad (A.14)$$

Neglecting terms in α^2 and higher, we have

$$\frac{\partial C}{\partial r} = -\alpha B - \alpha x \frac{\partial B}{\partial r}. \quad (A.15)$$

A solution to Eq. A.12 and Eq. A.15 may be written in the form

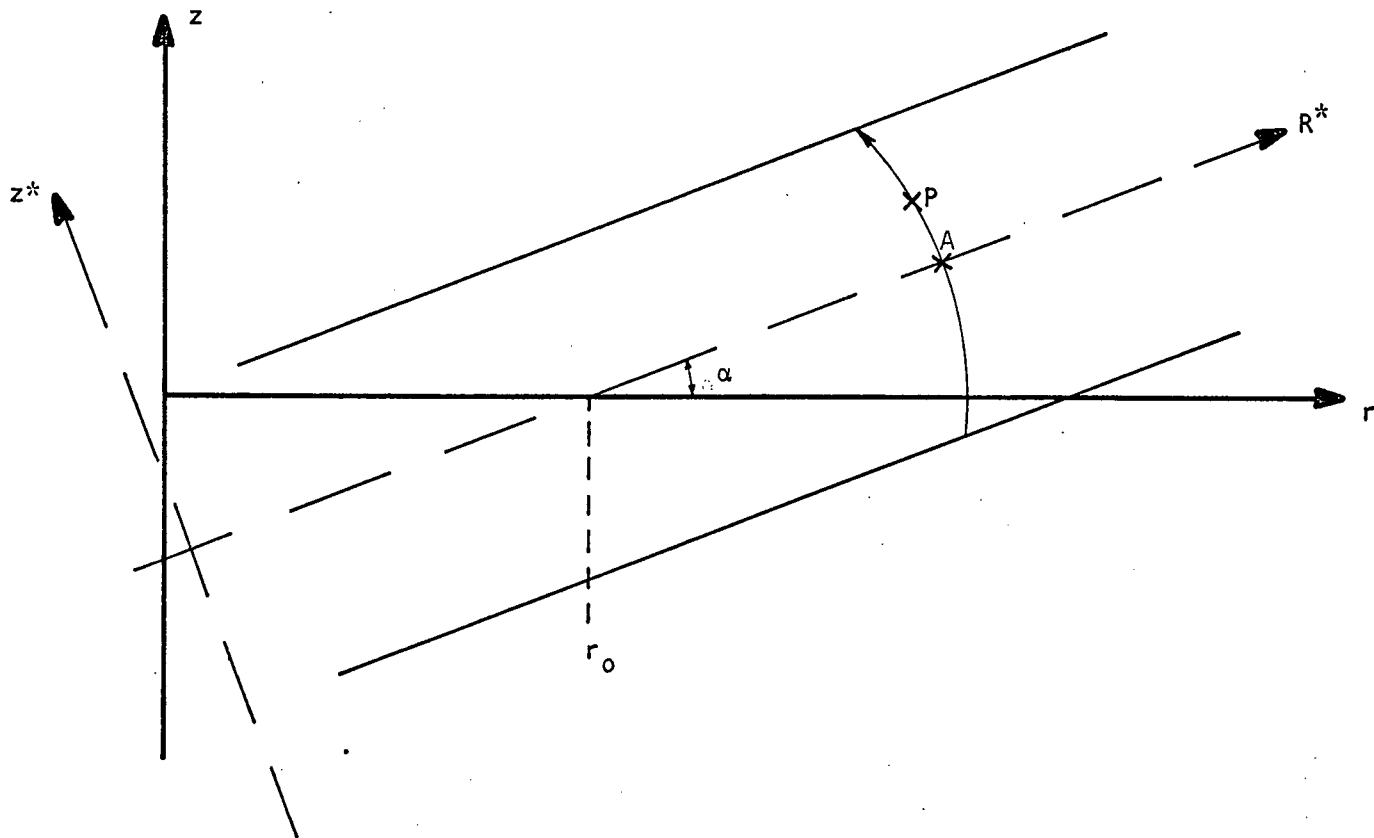


Fig. A.1. Tilted magnet sector parameters

$$C = -\alpha x B + \text{constant} \quad (\text{A.16})$$

or

$$C = Z_0^* B + \text{constant} \quad (\text{A.17})$$

where $Z_0^* = -\alpha x = (Z^* - z)$. Using this last expression for C , we can rewrite our Eq. A.6 in a form similar to Eq. 2.17. This shows that Eq. 2.17 can be used to gain a qualitative understanding of the effects of median plane misalignments. The discontinuities that occur in these expressions for the field components at the edges where the sectors are rotated would not occur in practice.